THE JOURNAL OF

Weather Modification

VOLUME 55, 2023 WEATHER MODIFICATION ASSOCIATION

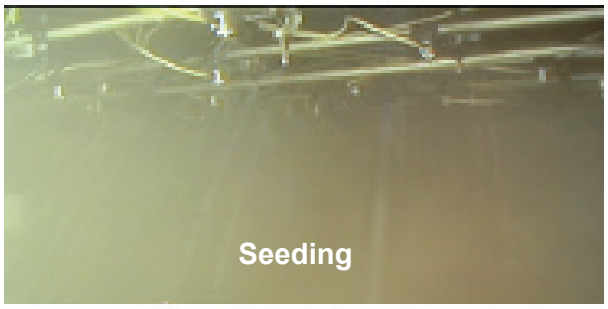

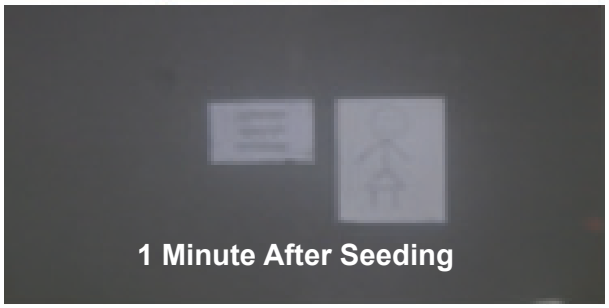

WEATHER MODIFICATION ASSOCIATION

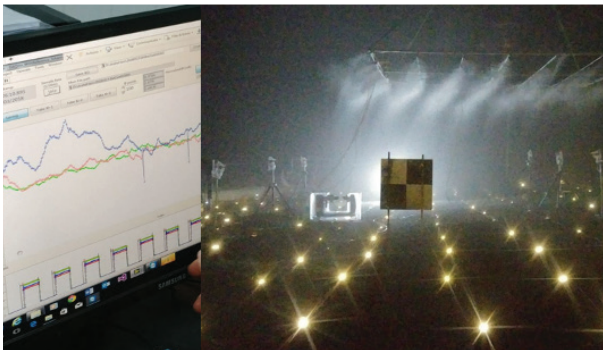

PROMOTING RESEARCH, DEVELOPMENT AND UNDERSTANDING OF WEATHER MODIFICATION FOR BENEFICIAL USES

Weather Modification Association

JOURNAL OF WEATHER MODIFICATION

EDITED BY:
Tom DeFelice, Editor

Erin Fischer, Editorial Assistant
EFISCH Graphic Design LLC
Fargo, ND 58102

PUBLISHED BY:
Weather Modification Association
Laurie Capece, Executive Secretary
PO Box 845, Riverton, Utah 84065 USA
Phone: 801-598-4392
Email: wmaexecsec@gmail.com

Membership information is available by contacting the WMA Association at the Riverton, Utah address shown above or by visiting www.weathermodification.org.

Current membership costs per year:

Corporate Member	$500
Individual Member	$100
Retired Member	$30
Student Member	$0
Honorary Member	$0

COVER PHOTO: Cover images submitted by Khain et al. as part of the technical submission titled ***Warm Fog Elimination by Seeding with Salty Drops: Experiments and Theory*** presented herein.

THE WEATHER MODIFICATION ASSOCIATION

The Weather Modification Association was organized in 1950 to develop a better understanding of weather modification among program sponsors, the operators and members of the scientific community. In 1966, the first suggestion for a professional journal was proposed and Volume 1, No. 1, of the Journal of Weather Modification was published in March 1969. This historic publication now includes 55 volumes (56 issues).

Originally called the Weather Control Research Association, the name of the organization was changed to the Weather Modification Association in 1967. During its long history, the Association has:

- Pressed for sound research programs at state and federal levels.
- Promoted a better understanding of weather modification for beneficial use.
- Acted as a disseminating agent for literature.
- Provided extensive testimony before many federal, state and local committees and agencies in regard to all aspects of weather modification research and operations.
- Assumed an active role in the promotion of policy statements concerning all aspects of weather modification.
- Developed active positions on ethics, minimum standards for operations, and a strong certification program for operators and managers.
- Published the Journal of Weather Modification, the only professional journal in the world totally dedicated to the operational, societal, economic, environmental, legal and scientific aspects of weather modification.

The Journal is published annually and papers are always welcome for consideration in either the reviewed or non-reviewed sections. A nominal charge of $100 per page published in the final double-column format of the Journal. This fee is charged for all papers, foreign and domestic.

Additional information on the individual classes of membership can be found in the Articles of Incorporation found at http://www.weathermodification.org.

Applications for membership on a calendar year basis, as well as additional information, can be obtained by writing to WMA at the permanent address of the Association:

WEATHER MODIFICATION ASSOCIATION
PO Box 845
Riverton, Utah 84065 USA
Phone: 801-598-4392
wmaexecsec@gmail.com
http://www.weathermodification.org

TABLE OF CONTENTS

President's Message

The years 2022-2023 have been busy for those working in weather modification. The stresses created by changing climate have increased interest in targeted enhancement of precipitation in many regions. Hail damage mitigation projects continue in North and South America, and in Europe and Asia. Most projects are operationally focused, based on well-accepted conceptual models of how cloud seeding can be used to modify precipitation processes. A few quantitative physical studies to support and improve these conceptual models are being conducted but more are needed. By increasing collaboration between different research groups around the world we can achieve more with our limited research resources. The Weather Modification Association fosters collaboration by connecting weather modification workers at our annual meetings and through publishing the Journal of Weather Modification. Please join with us in these activities to share ideas and improve our ability to work effectively with the atmosphere.

Andrew Detwiler
WMA President, 2023

Editor's Message

The JWM Volume 54, ended up with 2 items including the editor's message, as happened with JWM Volume 53. The near record low paper submission numbers continue. The hope is for more papers, without the need to include the editor's message over the next few years as we begin to move beyond the Covid-19 event and as the need for potable water begins to increase in social priority.

The journal is an integral part of the WMA! It facilitates the communication of our operational and developmental activities within and beyond our organization. Proceeds from the JWM support WMA activities. Please consider submitting a paper, for example a "short" contribution or technical note based on a paper presented at our WMA meeting, or an operational project report, converted to the JWM paper format. Each JWM scientific article, technical note/short contribution has a unique DOI tag giving it global visibility. If in doubt about whether a paper might be considered publishable, then send a quick query to the JWM editor. Submissions of scientific articles, technical notes/short contributions, and articles for the message section (i.e., President's Message, In Memoriam) are accepted year-round via the online system. We have also started looking at improving the on-line journal system.

Dr. Thomas P. DeFelice
WMA Editor, 2023

In Memoriam
Arnett Dennis
1927-2022

Arnett Stanley Dennis was born in a farmhouse in Arlington, Prince Edward Island, Canada in 1927. He was the seventh child of William and Ruth (Gorrill) Dennis. He began his formal education in the local one-room school. He graduated from Prince of Wales College in Charlottetown, Prince Edward Island in 1947, and from Acadia University in Wolfville, Nova Scotia in 1949. He later received M.S. and Ph. D. degrees in physics from McGill University in Montreal, Quebec. While living in Canada, Arnett worked at various times as a farm hand, public school teacher, surveyor's assistant, laborer in a copper refinery, weather forecaster at Royal Canadian Air Force stations, and as a radar meteorologist for McGill University. As he completed his Ph.D. studies at McGill the brand new field of weather modification was rapidly expanding and he was drawn into it.

Arnett moved to California in 1955 where he joined the Weather Modification Co. (WMC) of San Jose, California where he managed cloud seeding projects in California and several other states. He then went

Fig. 1. Arnett Dennis conduct a weather briefing for Hailswath in 1966. Photos courtesy of South Dakota School of Mines & Technology (SDSMT).

to work with the Stanford Research Institute (SRI) in Menlo Park, California where from 1960-1965, he led an early, theoretical study of the feasibility of observing rainfall from radar-equipped weather satellites and also took part in classified (secret) research for U.S. Government agencies.

He moved to the South Dakota School of Mines & Technology (SDSM&T) in Rapid City in 1965 where he became the associate director of its Institute of Atmospheric Sciences (IAS). There he took on the management of a number of cloud seeding and weather radar studies in South and North Dakota. Much of the funding came from the federal Bureau of Reclamation (USBR) Skywater Project. In the late 1960's and early 1970's the IAS had more than 50 employees and contractors involved in these studies. Several aircraft and multiple weather radars were deployed to support cloud seeding field projects in South and North Dakota. Personnel from the IAS were involved in several addition projects, including the National Hail Research Experiment in northeastern Colorado. In addition to his research activities Arnett taught graduate courses in the Department of Meteorology. His cloud physics course included discussion of cloud seeding concepts. He also supervised the research of several M.S.-level graduate research assistants.

From 1974 to 1981 Dr. Dennis was the director of the IAS and an ex officio member of the South Dakota Weather Modification Commission. This was a period of several significant challenges. One was battling the public perception that IAS cloud seeding experiments conducted over the plains east of Rapid City on June 9, 1972 contributed to heavy rains over the Black Hills, a dam failure, and a massive flood that swept through Rapid City later in the evening that caused the deaths of 238 people. This took significant effort by IAS leadership, including Dr. Dennis. Another challenge was the slow but steady reduction of USBR funding for IAS cloud seeding research projects beginning in the early 1970's. In response Arnett managed to guide the diversification of the IAS research portfolio into new areas. A third challenge was the demise of operational cloud seeding programs in South Dakota. This was driven by unfounded public perception that if cloud seeding leads to more rain falling in one place, then less rain will fall in neighboring areas with no cloud seeding. Other critics claimed that cloud seeding decreases precipitation. Despite great efforts from Arnett and his IAS colleagues these false perceptions proved too difficult to combat. There has been no operational cloud seeding in South Dakota since 1976.

During his time at SDSM&T Dr. Dennis also was a consultant to several scientific agencies, including the World Meteorological Organization (WMO). In 1978, on behalf of the WMO, he traveled alone through four French-speaking countries in West Africa, collecting information on their attempts to alleviate droughts by cloud seeding.

In 1981 Arnett moved to the U.S. Bureau of Reclamation (USBR) at the Denver Federal Center. His earliest work at the USBR also dealt with weather modification, but he later became involved in studies of the potential impacts of global warming on USBR water conservation projects in the western United States. He retired from federal service in 1991.

Fig. 2. Dick Schleusener, the Director of the Institute of Atmospheric Sciences at SDSMT and Arnett Dennis, Associate Director, attend the 1973 Weather Modification Association Annual Meeting.

In retirement Arnett put his talents to work in an active life of social and intellectual pursuits in the Rapid City area. He did some part-time teaching, served as an expert witness in legal cases, and contributed his energies to the activities of several local service organizations. He and his wife Maralee spent their later years in Rapid City at the West Hills Village Retirement Community.

Arnett was a Fellow of the American Meteorological Society, a member and past president of the Weather Modification Association (WMA), and a member of the Society of Sigma Xi / Research Society of America. His textbook Weather Modification by Cloud Seeding was published by Academic Press, New York in 1980 and in Russian translation in Moscow in 1983. It summarized knowledge about cloud seeding as of the late 1970's. It was quite popular and has been the only textbook on weather modification distributed world-wide by a major textbook publisher. He was the author of numerous scientific papers and reports, many of which he presented at national and international conferences. His work involved travel to about 20 foreign countries, including Iran, China, and

other former Union of Soviet Socialist Republics (U.S.S.R.), to meet with fellow scientists and other residents of these countries. His first visit to the U.S.S.R. in 1973 included a tour of the historic city of Samarkand in central Asia.

Dr. Arnett Dennis had a quiet patient manner when exchanging views on scientific issues. He rarely spoke without thinking beforehand and maintained great respect for different viewpoints. These elements of his character served him well through his long productive career.

ON THE IMPLEMENTATION OF RAIN ENHANCEMENT OPERATIONAL MANEUVERS USING UNCREWED AIRCRAFT SYSTEMS WITH AUTONOMOUS-ADAPTIVE TECHNOLOGIES*

T.P. DeFelice[1]

Aeronautical Engineering Sciences Department, University of Colorado Boulder, CO USA
[1]Current Affiliation: Science Systems and Application, Inc., Lanham, MD
[*]Parts of this paper were presented at the 2023 WMA Annual Meeting, Westminster, CO

1.0 INTRODUCTION

The research team implemented a framework involving an uncrewed aircraft system (UAS) with atmospheric and cloud microphysical sensing and autonomous adaptive control technologies that searched, identified, performed, monitored and evaluated cloud system candidates for successful cloud seeding operations to enhance precipitation using hygroscopic seeding agents. The implementation featured trials in the U.S. Great Plains area following U.S. Federal Aviation Administration (FAA) regulations during a three-week summer field campaign. The trials provide a demonstrated step toward the potential for improved seeding targeting efficiency, and hence improved operational cloud seeding activity effectiveness. The implementation of the integrated UAS provided and exploited the temporal and spatial cloud-scale sensitivities to overcome the operational and natural uncertainties, or sparseness of environmental attributes, needed to increase cloud seeding operational efficiency. The following sections provide some background (Section 2.0), followed by results of the field campaign and their discussion (Section 3.0). Then some closing remarks and a recommendation for future work (Section 4.0).

2.0 BACKGROUND

This project has roots from a 1985 winter season research project in northern Utah led by Dr. Geoffery Hill (Figure 1). That project involved setting up and implementing a balloon-borne system that carried a payload consisting of a modified standard U.S. National Weather Service-like rawinsonde unit with a vibrating wire device to provide water content particularly supercooled liquid water instead of its standard hygristor, and a miniature silver iodide (AgI) acetone solution generator. The rawinsonde data were sent to the rawinsonde tracking station located at the target area operations site. The sonde's vibrating wire output was converted to the amounts of supercooled water mass and sent to the rawinsonde tracking system. The sonde's temperature data were simultaneously sent to the rawinsonde tracking system and used to electronically activate the AgI solution generator. The seeding was initiated when the temperature was at or lower than 0°C (273 K) and the vibrating wire indicated increased mass. All system components were calibrated and worked in the operational environment. However, the seeding signature indicated by the change in ice crystal spatial density over the target area site was never confirmed. The most significant lessons learned were the importance of targeting of seeding material, followed closely by the ability to adequately observe the resulting effect. Additionally, a lesson learned exercise solution discussion indicated the need to have used a more controllable platform to achieve more successful results, namely a miniature uncrewed airplane to accomplish the goal of said project. The uncrewed airplane would have been able to hold a larger payload which could have included a video camera. Dr. Hill's program was one of many influences suggesting the need to instrument seeding aircraft

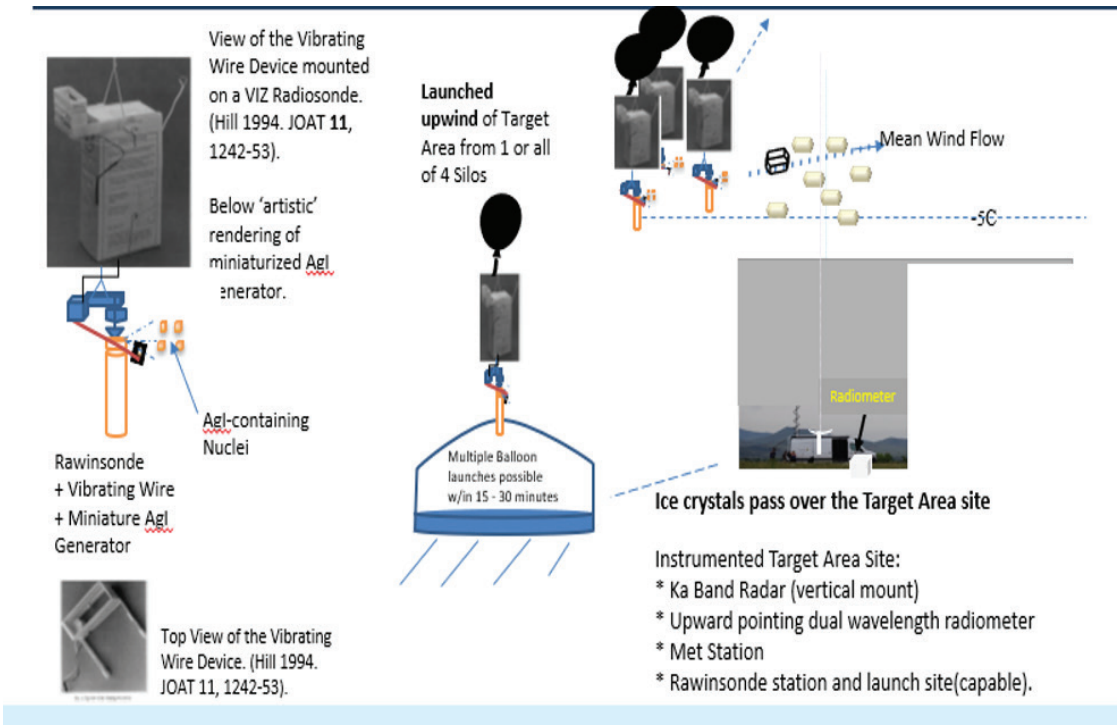

Fig. 1. Conceptual balloon-borne AgI-acetone solution generator attached to a modified rawinsonde that contained a vibrating wire device instead of a hygristor (left) to downwind of the launch site (center) to the target area site further downwind.

and the corresponding development and application of emerging technologies relevant to cloud seeding, and a continuing encouragement for using sensors on-board operational cloud seeding aircraft.

Correct targeting arguably remains the weakest link in cloud seeding operations, despite the overall improvement in modern cloud seeding technologies. The research team designed and implemented a project with the goal to develop and assess an engineering approach featuring an autonomous uncrewed aircraft system (or UAS) that utilizes local radar and data from UAS-mounted meteorological and microphysical sensors to identify a seedable cloud, determine when to seed that cloud, seed the cloud then evaluate the seeding result and repeat. The purpose of the field campaign was to evaluate the sensor and system components performance. It was a below cloud base only campaign, staying within FAA guidelines, using single and then dual UASs. The concept of operations was patterned after ASCE (2017), and contained the following significant steps:

Step 1: Perform system checks, communicate between UAS and ground control station and project stakeholders, receive radar coordinates.

Step 2: (Autonomously) Fly to and reach the Lifted Condensation Level (LCL). Measure meteorological; state parameters, wind field, aerosol concentrations (used as a cloud condensation nuclei CCN proxy) and droplet spectral concentrations at cloud base.

Step 3: Run Cloud Seed Algorithm (CSA) to calculate height and time of first drizzle, LCL, Seed/No Seed Decision.

Step 4: Implement maneuver(s) based on Seed/ No-Seed decision. (Repeat w/ 2 UASs).

The campaign would be successfully accomplished by satisfying the following key objectives:

1. Ensure quality output of the different system components, including from a manual input

2. Assess the performance of the improved Thunderstorm Identification, Tracking, Analysis, and Nowcasting (TITAN) software, and cloud seeding algorithm (CSA) (Hirst et al. 2023).

3. Perform operational evaluation of an UAS for targeting seedable clouds and Seed or Not Seed decisions within the regions of interest identified by the improved TITAN software.

4. Transfer the knowledge gained.

3.0 RESULTS AND DISCUSSION

The field campaign was proposed to be in the United Arab Emirates (UAE). COVID delayed the field campaign by about 2 years, which affected resource availability. Items that were affected included; UAS system component and entire system check completions, shipment date, time through customs in the U.S. and UAE. There were also contributing complications due to U.S. FAA and the UAE FAA-equivalent flight restrictions. The flights had to be within line of site, below cloud base and during daytime. The goal of the field campaign was to assess the potential utility of UAS that employ in-situ real-time data to support the autonomous decision to identify clouds likely suitable for cloud seeding using hygroscopic seeding agents in an operational field project environment. The field campaign was conducted in the U.S. Great Plains region after considering alternative locations. There were 9 flights total. These flights collectively covered all project objectives multiple times (5 for single UAS, 4 dual UASs).

The daily routine started with a morning forecast brief and discussion, operations status, plan for the day with a late afternoon follow-up, all very similar to the conventional standard practice document (ASCE 2017). The dual aircraft flights utilized one UAS to identify a seedable area, UAS (Obs), and the other to carry out the seeding, UAS (Seed). The UAS is shown in Figure 2. UAS (Obs) is a Super Raaven airframe with a 4.9 m wingspan, and a tail to front edge length of 1.5 m, excluding the sensor. This UAS held a miniaturized Cloud Droplet Probe (CDP), Multi-angle Inertial Probe (MIP), and Portable Optical Particle Spectrometer (POPS). UAS (Obs) had a gross takeoff weight of 13.6 kg with up to 2 hr. of endurance at a cruise speed of 16 m/s. UAS (Seed) is a Raaven airframe chosen for its durability and its quick launch capability (e.g., Frew et al., 2020). Both UASs are shown in Figure 2. UAS (Obs) has up to a 3-hr. endurance at a cruise

Fig. 2. The two Uncrewed Aircraft Systems used for the research project UAS (Seed) is on the right side and UAS (Obs) is on the left side of the figure. The flight crew with ad hoc team members shown. Photo courtesy of Alex Hirst.

speed of 17 m/s and a wingspan of 2.3 m. UAS (Seed) holds the seeding dispensing system and had the same avionics and flight sensors as UAS (Obs). The seeding dispensing system was designed to release hygroscopic seeding agents near cloud base from three tubes each capable of holding 1 kg of material independent of form (e.g., particles including nanoparticles) per the directed requirement. UAS (Seed) also maintained altitude and distance offsets throughout its flights to ensure UAS (Seed) was nearby and could quickly begin seeding operations identified by UAS Obs). This functional division allowed for seeding and evaluation to happen near simultaneously. It also allowed for the evaluation of the seeding to continue and the transition to search as needed while the UAS (Seed) drone landed and returned to operations as needed. Axisa and DeFelice (2016), Hirst et al. (2023) and DeFelice et al. (2023) provide additional UAS details.

The August 28, 2021 flight (#9) is used as a representative example for a dual UAS mission (Figure 3). The autonomous control was engaged except for the short period between t≈4100 to ≈4400 seconds into the flight, and at the end of the flight. This flight had three operational regions of interest (ROIs) provided from the local radar fed improved TITAN software the research team denoted as RECCES, which contains the cloud seeding algorithm (CSA). Immediately following the report of a seedable location, i.e., the initial Fly to Seed Point (FTSP), UAS (Obs) climbed away from the identified seedable location) and headed downwind before entering a specific evaluation trajectory. Meanwhile, UAS (Seed) completed the current commanded flight trajectory or state maneuver first. Then it proceeded autonomously to the identified seedable point (FTSP) where it then autonomously entered the 'Release Seed Material' or 'RSM1 (Figure 3)' state and followed a seeding trajectory. Once seeding ended the UAS (Seed) then autonomously descended and entered a 'loiter' trajectory to await future commands ('Loiter' state).

The length of, or time to complete, the 'Release of Seeding Material' segments vary and were related to the wind field and progress made through the existing commanded flight trajectory; Similarly for the length of the 'Fly To Seed Point' except there was no delay in its start upon its receipt. Other

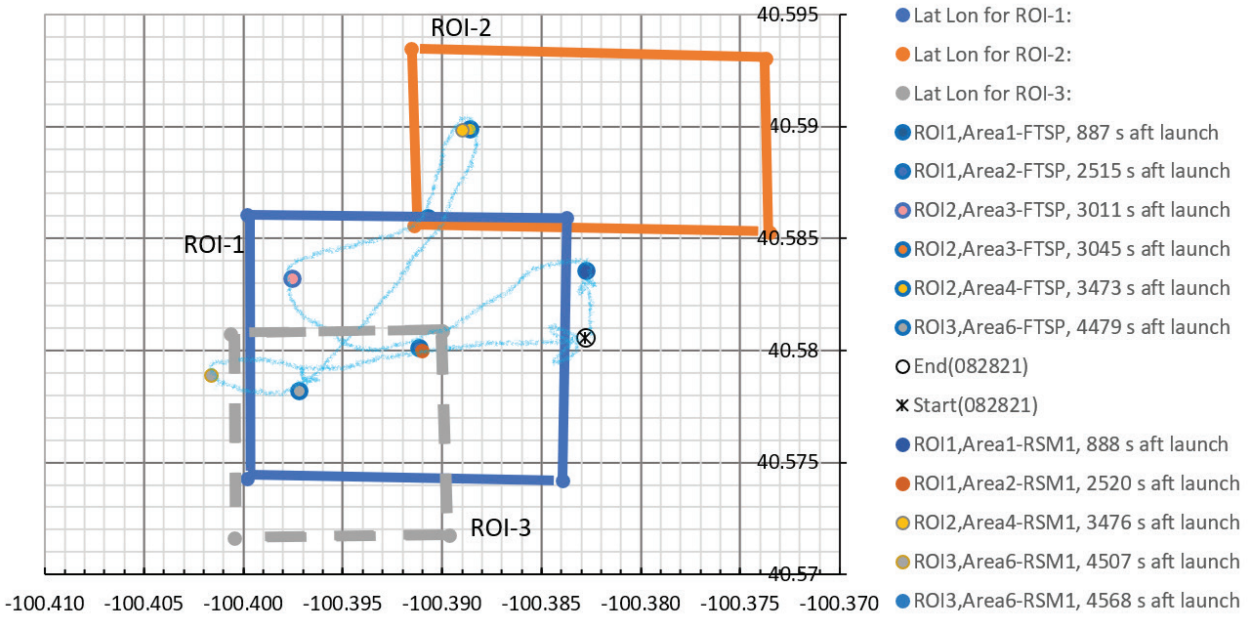

Fig. 3. The streamline path flown by UAS (Seed) from launch to land (grey trace originating at the start/stop point location, (40.805° and -100.3825°). Also shown are the locations of the initial 'Fly to Seed Point' or 'FTSP' state and the initial 'Release Seeding Material' or 'RSM1' state traces during the August 28, 2021, dual UASs flights.

contributing factors to the length of, or time to complete, a commanded trajectory include ensuring no damage to the UAS or flight crew, and fulfilling a contract deliverable, e.g., demonstrating the ability that allows operator inputs should the need arise.

The RSM1 points in Figure 3 are mostly in the ROIs, except for the initial point and the point at 4507 s following launch. Hence, the research team accepted that seedable clouds susceptible to seeding to impact the warm rain process were found within the ROI. Given the proximity of the initial point and time for an effect to occur, if the wind field was into the ROI, then seeding would possibly have been initiated in a conventional seeding operation. Such could have been accomplished in this campaign by testing the interface allowing for manual input, which was not done. However, such a test was done while waiting for the ROI-3 coordinates and to ensure the UAS remained FAA compliant while testing the profile maneuver between ≈4100 to ≈4400 seconds into the flight. The dual UAS's, after the profile test ended, received the ROI-3 coordinates and autonomously repeated the maneuvers, i.e., go to the ROI-3 (Area 6), search for seedable conditions, initiate seeding if the onboard sensors so indicated and evaluate after which they were to loiter. During loiter, having completed all field campaign objectives and since the effects from the forecasted frontal boundary had begun to enter the operational area, both UASs were commanded to return to base.

The research team investigated how close to the metric spectra for initiating the warm rain processes were observed from the aerosol spectra when the CSA outputted "Cloud Seed Flag=1, or at the initial 'Fly To Seed Point (FTSP)' through Release Seeding Material (RSM1) maneuver sequence (Figure 4). The dashed rectangle represents the tail in the spectra associated with initiation of the warm rain process. The more predominant the spectra are in this region the greater the probability of a successful seeding effect. The UAS (Obs)

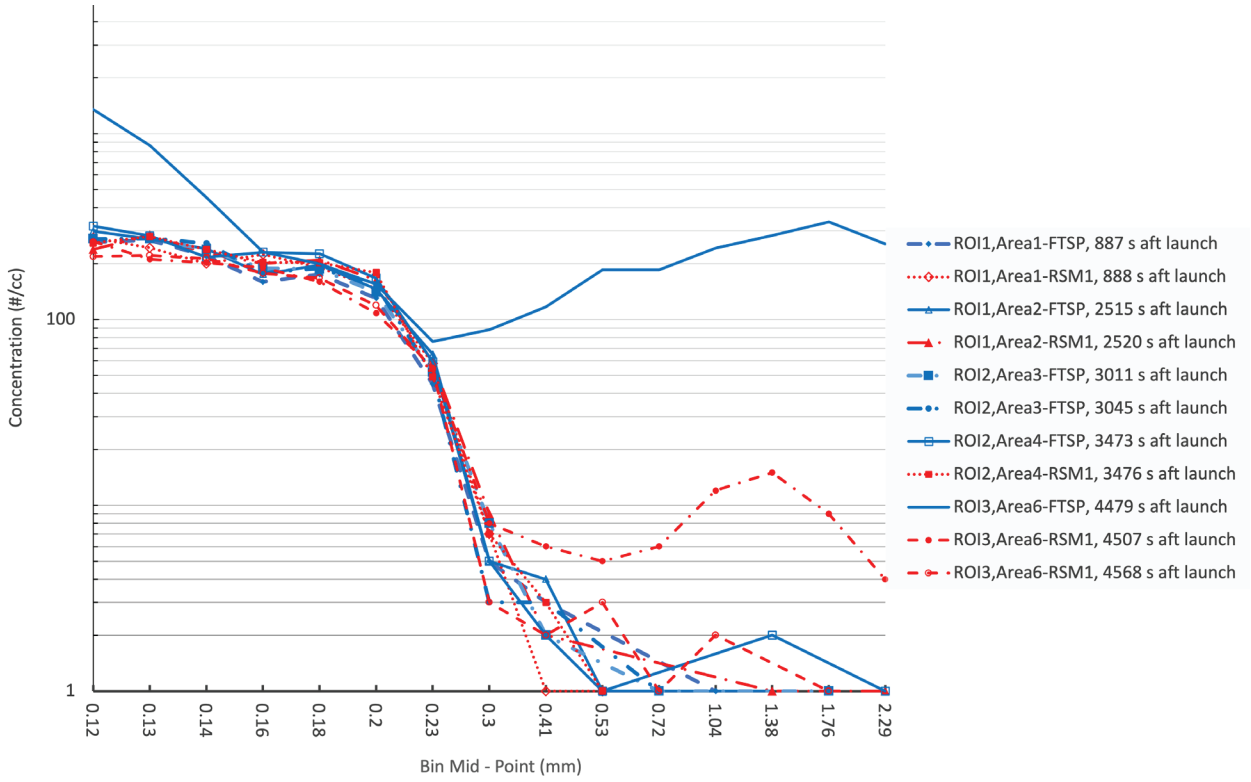

Fig. 4. Aerosol concentration (#/cm^3) plotted versus dSize BINiameter. Size BINs 1 through 15 represent averaged mid-range diameters (microns) of 0.13, 0.14, 0.16, 0.18, 0.2, 0.23, 0.3, 0.41, 0.53, 0.72, 1.04, 1.38, 1.76, 2.29, 2.98, respectively.

and UAS (Seed) are generally further apart at the RSM1 location where the seeding starts compared to at the initial FTSP state, except when observed in the vicinity of an approaching frontal boundary or greater storm dynamical region, such as in the case of the ROI 3 spectra locations. One spectrum was tied to the point whose tail stopped at or was just left of the dashed oval, generally indicating that local area was not conducive for seeding and its CSA Seed flag was 0.

The evaluation of the cloud seeding effect from hygroscopic seeding is complex and would still require the application of strong physical and statistical techniques. The mobile operational center approach and the on-board UAS sensors are helpful. However, it is unclear how to accomplish seeding maneuvers if they involve cloudy air, given current FAA visual drone flight rules. The mobile operations center allowed the team to maintain line of sight with a UAS as it flew toward the downwind storm direction ultimately to intersect with the affected seeded cloud as long as it is in and remains within the region of interest. The on-board sensors would also have measured the history of the aerosol and hydrometeor size spectra throughout its flight, enabling the analysis to distinguish a different than background aerosol and droplet spectra (i.e., a possible seeding signature).

4.0 CLOSING REMARKS

An uncrewed instrumented aircraft successfully identified seed/no seed targets (cloud systems) in a manner equivalent to the current standard practice (ASCE 2017) but with limited, if any, human input(s), simply using onboard sensors and ancillary radar, and a non-conventional mobile operations center. This study has demonstrated the feasibility of using UASs to carry out cloud base seeding of warm clouds (i.e., clouds whose temperatures are entirely above freezing) while observing current FAA regulations. A benefit compared to the current standard practice is the potential for improved targeting efficiency and therefore higher confidence of the seeding effect.

There is still a lot of developmental work to complete before achieving an operational readiness level of this UAS application; flight aviation regulations notwithstanding. For example, besides the continued development to improve targeting efficiency for warm cloud seeding, work is needed to document possible extra area effects from using hygroscopic seeding agents (Silverman 2003; Rosenfeld et al. 2010; DeFelice et al. 2014; Gayatri et al. 2023). It is recommended that follow-on experiments be conducted as part of larger operational cloud seeding projects that may benefit from the results of this study (DeFelice et al. 2023).

5.0 ACKNOWLEDGMENTS

The author recognizes and appreciates his research teammates for their roles played in the successful completion of this project, namely; Duncan Axisa (CW3E, UCSD), John J. Bird (UTEP), C. Alexander Hirst (CUB), Eric W. Frew CUB), Roelof. P. Burger (N-W Univ), Darrel Baumgardner (Droplet Measurement Technologies, LLC), Gerhard Botha (N-W Univ), Henno Havenga (N-W Univ), Dan Breed (NCAR, RAL retired), Steve Bornstein (University of Colorado Boulder, CUB, Integrated Remote and In Situ Sensing, IRISS; CUB-IRISS), Chris Choate (CUB, CUB-IRISS), Ceu Gomez-Faulk (CUB-IRISS), Michael Rhodes (CUB-IRISS) for their efforts to ensure a successful project This work was funded by the National Center of Meteorology, Abu Dhabi, UAE, under the UAE Research Program for Rain Enhancement Science (UAEREP) and the University of Colorado (CUB), CUB-IRISS. Thanks to Don Griffith for the excellent review of this paper. Any mention of commercial instruments, hardware, software, or systems in this paper does not imply endorsement by the authors, nor their employers, nor the funding agency as the actual performance depends on the application and the system-wide requirements.

6.0 REFERENCES

ASCE, 2017. ANSI/ASCE/EWRI Standard Practice 42-17, Standard practice for the design, conduct, and evaluation of operational precipitation enhancement projects. DeFelice, T.P., Ed. ASCE, Reston, VA pp. 52, http://ascelibrary.org/doi/book/10.1061/9780784414408.

Axisa, D., DeFelice, T.P., 2016: Modern and prospective technologies for weather modification activities: a look at integrating uncrewed aircraft systems. Atmos. Res. 178–179, 114–124.

DeFelice, T.P., Axisa, D., 2016: Developing the Framework for Integrating Autonomous Unmanned Aircraft Systems into Cloud Seeding Activities. J Aeronaut Aerospace Eng, 5, 172, https://doi.org/10.4172/2168-9792.1000172.

DeFelice, T.P., Axisa, D., 2017: Modern and prospective technologies for weather modification activities: Developing a framework for integrating autonomous unmanned aircraft system. Atmos. Res. 193, 173-183, https://doi.org/10.1016/j.atmosres.2017.04.024.

DeFelice, T.P., J. Golden, D. Griffith, W. Woodley, D Rosenfeld, D Breed, M. Solak, B. Boe, 2014: Extra area effects of cloud seeding - an updated assessment. Atmos. Res., 135-136, 193-203.

DeFelice, T.P., Axisa, D., Bird, J., Hirst, C.A., Burger, R., Baumgardner, D., Frew, E., Botha, G., Havenga, H., Breed, D., Bornstein, S., Choate, C., Gomez-Faulk, Ceu, Rhodes, M., 2023: Modern and Prospective Technologies for Weather Modification Activities: A first demonstration of integrating autonomous uncrewed aircraft systems. Atmos Res. 1-12, 90, https://doi.org/10.1016/j.atmosres.2023.106788.

Gayatri, K., Prabhakaran, T., Malap, N., Konwar, M., Gurnule, D., Bankar, S., Murugavel, P., 2023: Physical evaluation of hygroscopic cloud seeding in convective clouds using in situ observations and numerical simulations during CAIPEEX, Atmos. Res. 284, 106558, https://doi.org/10.1016/j.atmosres.2022.106558.

Hill, G.E., 1994: Analysis of Supercooled Liquid Water Measurements Using Microwave Radiometer and Vibrating Wire Devices. J Atmos Oceanic Tech 11, 1242-1252, https://doi.org/10.1175/1520-0426(1994)011<1242:AOSLWM>2.0.CO;2.

Hirst, C. Alex, Bird, J., Burger, R., Havenga, H., Botha, G., Baumgardner, D., DeFelice, T.P., Axisa, D., Frew, E., 2023: Field Deployment of an Autonomous Uncrewed Aircraft System Performing Targeted Atmospheric Observations. Field Robotics May, 2023(3), 687–724, https://doi.org/10.55417/fr.2023022.

Rosenfeld, D., Axisa, D., Woodley, W.L., Lahav, R., 2010: A quest for effective hygroscopic cloud seeding. J. Appl. Meteorol. Climatol. 49, 1548-1562.

Silverman, B. A., 2003: A critical assessment of hygroscopic seeding of convective clouds for rainfall enhancement. Bull. Amer. Meteor. Soc. 84, 1219–1230.

A LABORATORY INVESTIGATION OF THE EFFECT OF HYGROSCOPIC AEROSOLS OF VARIOUS ORIGINS ON CONTROLLED CLOUDY ENVIRONMENTS

A Collaborative Effort from the Scientists and Engineers of:

Cloud Seeding Technologies, Gaertringen, Germany

ABSTRACT

The article is an examination of an experimental study of the interaction of hygroscopic aerosol particles of various origins, particularly thermocondensation variant and mechanically destroyed (pre-prepared powders), with a warm cloudy environment ($T \geq 273$ K). Depending on the concentration, properties, and spectrum of the aerosol used, as well as the structure of the colloidal cloud medium, the result of the interaction can be a stabilized and/or destabilized form of the latter. Our experimental results have shown no consensus on whether the variant from exposing standard pyrotechnic flares equipped with a composition that generates a hygroscopic-variant aerosol to destabilize the colloidal stability of the cloud media, and, accordingly, can lead to an increase in precipitation. The authors believe this is due to the significant uncertainty in the processes of aerosol formation, both in the process of laboratory experiments and directly during cloud seeding operations.

1.0 EXPERIMENTAL SETUP

The experiments were conducted using equipment that simulated actual environmental conditions to the maximum extent possible. The equipment consisted of a cylindrical cloud chamber with a height of 18 m, and a radius of 7.5 m to constitute a volume of 3200 m^3. The chamber is capable of an atmospheric pressure range from 1 – 2.5 atm and is designed to simulate and observe cloud physics in a controlled environment. The operation of the generator in the natural environment is simulated in a horizontal wind tunnel with air blowing at a speed representative of real environmental conditions of a generator in operation. Next, a representative sample of aerosol from the wind tunnel path is introduced into the cloudy environment formed in the climatic chamber.

The cloud in this study was simulated by adiabatically cooling the enclosed chamber air with a known initial humidity and aerosol background to simulate the formation of a natural cloud in an ascending air flow[1]. To simulate a convective cloud, a uniform pressure release was maintained to simulate the rise of an air mass at a speed of 2 m/s. For stratus clouds, a pulse of pressure reduction was used, and the appropriate pressure maintained to achieve the formation of the desired concentration of drops. During the experiments, the main environmental physical state, meteorological parameters including updraft velocity, cloud drop concentration and size spectra, were monitored using standard commercial sensing devices inside of the chamber as described in Section 2.2. The amount of water deposited on the test sites was measured continuously by a scale to monitor the weight of water precipitating onto a 1 m^2 collection membrane placed in the chamber in a location representative of the natural ground.

2.0 METHODOLOGY

2.1 Physical basis of seeding clouds with hygroscopic aerosols.

The main application of hygroscopic aerosols is to affect warm clouds ($T \geq 273$ K). There are two variants of functional manifestations of hygroscopic

[1] The terminology 'air flow' and 'air speed' are used in this text in place of 'wind speed' because the experiments take place within a controlled chamber environment.

aerosol, implemented separately or jointly.

1. **Thermodynamic effect**. Since the process of water adsorption by aerosol particles is associated with some heat release, the introduction of a hygroscopic aerosol could enhance the buoyancy of the cloud system sufficiently. The consequence of this phenomenon is that the cloud will develop to reach a level above the freezing point. An increase in the optical density of the system and, accordingly, radiation heating also contributes to this process. In this case, we can state the further formation of sediments by the glaciogenic mechanism.

2. **Change in the colloidal stability of the system.** The second option is directly related to changes in the particle size of a hygroscopic substance due to water adsorption, and changes in the dynamics of processes taking place in a colloidal medium which mainly affects the various mechanisms of coagulation (gravitational, turbulent, Brownian, electrostatic). Unlike the previous version, this process can lead to a change in the state and stability of the colloidal system, which can be identified by both an increase and a decrease in precipitation.

Reagents used in this research:

Multiple substances, including NaCl and $CaCl_2$ are considered. When water is absorbed by a hygroscopic substance - cloud condensation nuclei (CCN) - we consider the following stages:

1. Rapid water absorption. In terms of energy and bond strength, this stage is comparable to a chemical reaction – for example in practice, compounds like $CaCl_2$, $CaCl_2$ * $4H_2O$, $CaCl_2$ * $6H_2O$ should be considered different substances.

2. Fast transition from a solid to a state of concentrated solution. The state of the process at this moment is determined by the Van't Hoff factor associated with the number of initial molecules and degree of dissociation of the substance and therefore associated with the chemical nature of a particular substance.

3. The area of dilute solutions, for which Raoult's law is valid, according to which the partial vapor pressure over the solution is also proportional to the molar fraction and degree of dissociation of the given substance. Accordingly, at this stage of dilution, the physical and chemical features of specific substances do not affect the vapor pressure of water over the solution.

4. With further dilution, the concentration of the solute becomes too low, and the drop of solution does not differ in properties from the rest of the droplets of the cloud medium.

In traditional warm cloud seeding operations applied to convective clouds, hygroscopic aerosols ascend within an air flow until the air reaches the condensation zone, typically at or just below cloud base. In this situation it should be noted that the stages of chemical bonding of water vapor molecules with a hygroscopic substance through its transformation into a solution drop happens very quickly when humidity is close to 100%. The growth rate from a drop of concentrated solution to a significantly more diluted, typical sized cloud drop is also rapid, rendering the chemical composition physically insignificant. While environmental considerations are beyond the scope of this research, logic suggests using the most environmentally sound, worker and economically friendly hygroscopic agents.

2.2 Change in the colloidal stability of a cloud system upon introduction of a hygroscopic aerosol.

Depending on the size and concentrations of the aerosols generated, the change can occur in two directions - an increase in the stability of the system or its destruction. In the actual environmental situation a wide range of aerosol sizes must be considered, this leads to the simultaneous implementation of two opposite mechanisms.

Accordingly, the outcome will depend on which mechanism is predominant. This situation, from the point of view of the authors, takes place in all cases - both for the aerosol produced during the combustion of pyrotechnic compositions, and in the case of the dispersal of pre-prepared powders.

The following options for introducing aerosol were used: pneumatic spraying of pre-prepared powders into the volume of the chamber, burning small amounts of pyrotechnic compositions under conditions simulating a real airflow, as well as burning full-size pyrotechnic generators (Burn-In-Place Flares) in a horizontal wind tunnel with the introduction of a representative aerosol sample into the chamber. The spectra of aerosols of various origins were recorded by an electrostatic aerosol classifier of the TSI 3080 system and Laser Aerosol Spectrometer TSI 3340 manufactured in the USA are shown in Figure 1.

Considering the impact of a hygroscopic aerosol with a cloudy environment, two groups of effects are distinguishable:

1. The rain embryo effect: CCN with a diameter of more than 1 μm are introduced, respectively, when water vapor is absorbed, droplets are formed that are an order of magnitude, or more, larger than the size of the original aerosol. In this situation, the effect of various mechanisms of coagulation presides. (Rosenfeld 2010)

2. The competition effect: In the case of greater hygroscopicity compared to nature, the process of water adsorption prevails on the injected aerosol. In this case, under certain conditions, colloidal structures with different stability can occur. The development of this effect can both reduce the formation of precipitation in the case of a submicron aerosol and increase it in the case of a micron aerosol.

Our scientists believe that these effects are the interaction of the aerosol formed under the conditions of a specific air speed, and a specific spectrum with a two-phase medium.

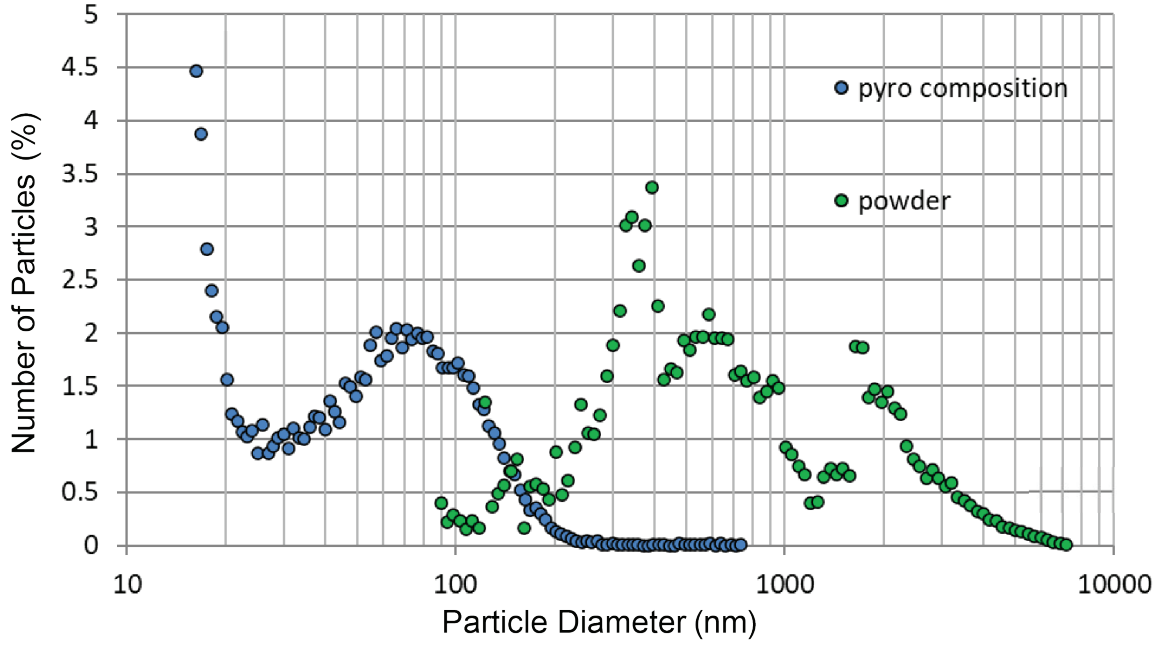

Fig. 1. Aerosol Spectra used in the experiment. Aerosol of pyrotechnic composition (composition described in the article ICE flares, blue dots) and aerosol obtained by pneumatic spraying of pre-prepared powder (NaCl with anti-caking additives). In both cases, the generator was in an air stream at a speed of 80 meters per second. From the point of view of the authors, in the second spectrum, the submicron size range is represented mostly by particles of an anti-caking additive that does not exhibit hygroscopic properties.

Since the formation of precipitation in a cloud occurs with the appearance of droplets larger than 30 μm in diameter, an increase in the amount of precipitation can be achieved by introducing particles larger than 1 μm into the cloud (e.g., DeFelice and Axisa 2017; DeFelice et al. 2023). Only such particles (or larger ones) can form the nuclei droplets which become raindrops. Nuclei with a diameter of less than 1 μm more likely perform the opposite function based on this and other hygroscopic seeding experiments like those conducted by Murakami et al. 2011.

Considering the effect of the real interaction of an aerosol with a cloudy environment, it should be considered that we are dealing with a spectrum formed as a result of a combination of the following processes:

1. Pyrotechnic aerosol - processes of condensation, coagulation, as well as changes in the chemical and physical properties of the formed aerosol.
2. Aerosol obtained by atomization of powders - physical destruction processes and powder dispersion under specific conditions of use.

2.3 Insertion of hygroscopic pyrotechnic aerosols to the cloud environment.

It should be noted that in the first case, the case of pyrotechnic flares, there are fewer opportunities for obtaining adequate information about the real environmental conditions while using generators. As a result, the information obtained by different researchers about similar compositions of Hygroscopic Burn-In-Place Flares differs significantly, but in almost all cases the percentage of droplet-forming particles larger than 0.9 – 1.0 microns is insignificant (Table 1).

It should be noted that in all observed studies, flares of approximately the same configurations were investigated – a charge diameter of 60 ± 10 mm, with a length of 120 – 300 mm, and in all the noted cases, similar compositions with minor deviations were examined: Potassium perchlorate ($KClO_4$) 65%, Hydrocarbon binder 18%, Sodium chloride (NaCl) 10%, Magnesium powder (Mg) 5%, [2]Lithium carbonate (Li_2CO_3) 2%; this conventional composition will be referred to as simply the Basic Reagent Composition or 'BRC'.

The numerous studies that have been conducted previously were done under different air speeds and other environmental variables making it impossible

Table 1. Comparison of aerosol spectra obtained by different research groups.

Information Source	Flare Composition	Air speed	Result
Zhengjun Su	n/a	n/a	70% < 0.5 μm
Rosenfeld D	South African Flare	Variable flight speed	99.5% < 1 μm
A. C. William, T.B. Roelof	South African Flare	90 m/s	mean diameter of particles 0.3 μm
R. T. Bruintjes and all	South African Flare, French Flare	30 to 40 m/s	Average diameter of 0.3 to 0.8 μm
M. Murakami	$CaCl_2$, $NaCl_2$ flares	n/a	Average diameter of 0.5 to 0.8 μm
WF-1 Airborne Pyrotechnic Flare Seeding System	Mg, KCl, $CaCl_2$, $KClO_4$ and Li_2CO_3	100 m/s	0.14% of particles with a diameter greater than 0.9 μm
Adapted from Haryanto, U., R. D. Goenawan, and D. Harsanti	South African Flare	n/a	1.1 – 2.1 μm

to draw conclusions from the multitude of studies on hygroscopic BIP flares.

The factors affecting the size spectrum are studied in detail in the next section.

Factors Determining the Spectrum of the Pyrotechnic Aerosol.

The authors studied the following factors, the influence of which to some extent determines the spectrum of the resulting aerosol:

- The composition of the pyrotechnic mixture.
- Flare design, including the effect of the generator wall on the spectrum of the resulting aerosol.
- The speed and direction of the airflow at the combustion front.

2.3.1 The composition of the pyrotechnic mixture.

We have studied four compositions that are very different from each other both in terms of combustion temperature and in terms of boiling points of high-boiling components:

1. The pyrotechnic composition of the US aircraft hygroscopic generator (BRC - #1).
2. Composition developed by the authors for the processes of stabilization of warm cloudy environments: based on a hydrocarbon binder and $KClO_4$ composition.
3. Classical pyrotechnic ice-forming composition (~12% AgI Composition).
4. Pyrotechnic composition of white smoke (KNO_3 70% Lactose 30% also known as "Rocket Candy").

The results of studying the aerosol spectra of the listed compositions are given in Table 2.

Despite the enormous difference of more than 1000 K in the combustion temperatures of the composition, and the difference of more than 2000 K of the boiling points of high-boiling components, the difference in the modal dimensions of the aerosol, and in the spectrum as a whole is quite small.

2.3.2 Flare design:

The spectrum of the formed aerosol depends both on the diameter of the flare and on the design features of the flare - primarily the presence of a wall and wall material. If in the case of diameter there is an almost linear dependence of the modal size on the diameter of the flare (Figure 2), then the effect of the wall is more complex.

Generally during combustion of a flare, the spectrum and amount of the resulting aerosol change as the combustion front moves deeper into the flare body,

TABLE 2. Investigation of the aerosol spectra of smoke compositions. Diameter of pyrotechnic material: 18mm, air speed: 8 m/s. Calculation of the content of the condensed phase in burning products and burning temperature under normal conditions and burning temperature performed using the "Astra-4" program.

# Composition	% Solid phase	Main condensed products	Estimated combustion temperature, K	Boiling point of high-boiling components, K	Modal aerosol size, nm
1	54	KCl, KOH, KO, $MgCl_2$, MgO, MgOH, NaCl, LiCl	2932	3873	124
2	41	KCl, KOH, KO	2801	1693	106
3	53	AgI	1860	2162	117
4	74	KO, K_2O, KOH	2968	1047	135

[1] Lithium chloride is the main product of the decomposition of lithium carbonate during combustion in the presence of a large amount of potassium perchlorate. For many reasons the authors have abandoned the use of lithium salts in formulations for environmental application.

while the process of aerosol deposition on the walls develops, the greater the deposition area and the greater the wall cooling rate by the oncoming air flow. In certain cases (non-combustible wall, relatively low burning rate and temperature of the pyrotechnic composition, high speed of blowing the flare with incoming cold air), more than half of the condensed phase may remain on the wall of the torch in the form of ash residue or condensed slag.

It should be noted that in the case of a non-combustible wall it is extremely difficult to model the processes occurring in real conditions during cloud seeding. The authors once witnessed a situation in which a hygroscopic composition with a very high content of ballast substances (more than 15%) and, accordingly, low energy characteristics, forming on the ground under experimental conditions a condensed phase that completely turns into an aerosol, caused a significant deposition of the condensed phase on the walls of the generator, up to complete overlapping of the generator tube in real flight conditions. This may have happened due to a combination of a significant cooling of the flame wall by a cold oncoming air flow and a slight decrease in the combustion temperature of the pyrotechnic mixture under conditions of lower atmospheric pressure. In this case, more stable results are obtained when burning flares with a completely combustible body, when there are no reasons for the deposition of the condensed phase on the walls, due to the absence of the latter (Figure 3).

2.3.3 The speed and direction of the airflow around the flare.

According to our studies, the speed of the air around the combustion front of the flare has the greatest influence on the aerosol spectrum. We have studied the aerosol formed during the combustion of a model generator equipped with the composition Hygroscopic Burn-In-Place Flares are used in the USA, Indonesia, Bulgaria, United Arab Emirates, etc. (Haryanto et al. 2011).

The diameter of the studied generator was 63.5 mm; combustion was carried out in a wind tunnel; the air speed was controlled from 5 to 80 m/s with an accuracy of 1 m/s. To eliminate the influence of near-wall flare effects, the sampling and analysis of an aerosol sample takes place during the first 20 seconds from the beginning of the flare burning. The results aerosol spectra and the dependence of the modal diameter on the velocity of the blowing flow are shown in Figures 4 and 5.

Summarizing the information obtained, it should be noted that the change in the modal size and spectrum of the hygroscopic aerosol depends on variations in the composition and design of the flare to a much lesser extent than on air speed relative to the combustion zone. According to our studies, the change in the modal size depending on the composition used does not exceed 30 nm, the influence of the flare diameter in the entire reasonable range of

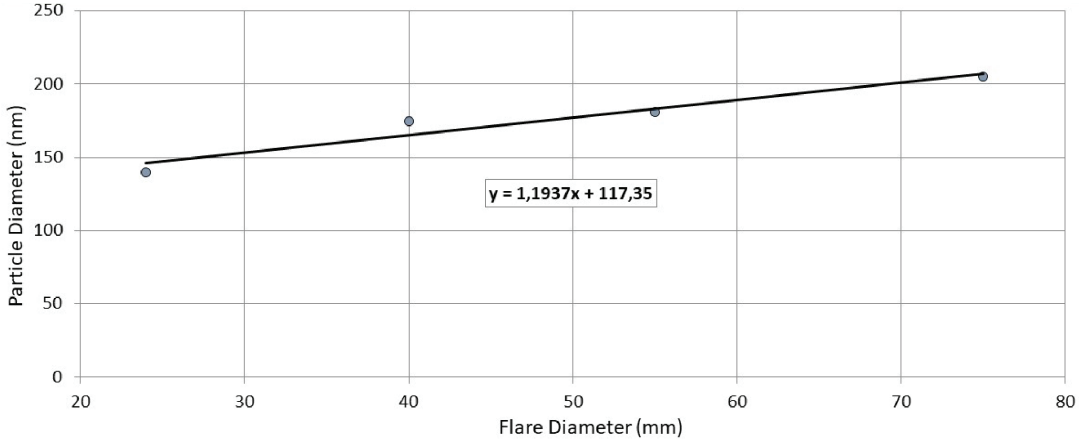

Fig. 2. Variation of the modal size of the aerosol depending on the diameter of the pyrotechnic charge (flare). Airflow speed 30 m/s, composition #1. The combustion of the composition without a shell.

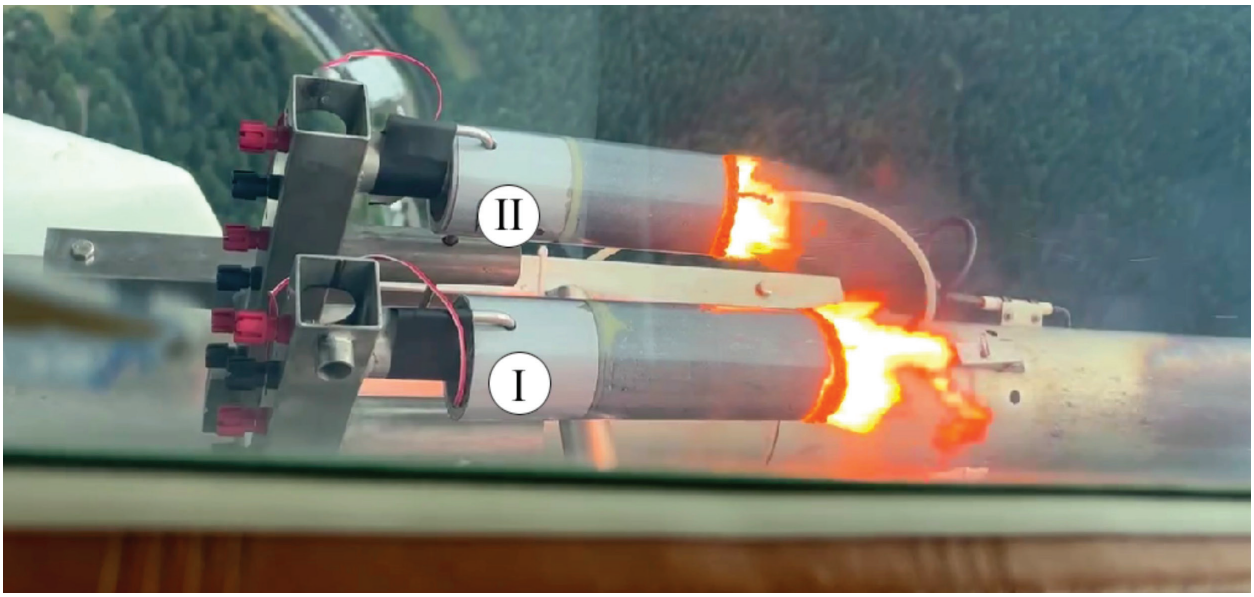

Fig. 3. Burning flares with an abnormally high content of calcium chloride in an easily combustible hull during flight.

sizes does not exceed 50 nm, while the change in air velocity in the speed range of 5-150 m/s leads to a change in the modal diameter by 200 nm.

Although the studied processes make it possible to change the spectrum of the formed aerosol, it is not large enough to reach the sizes of the micrometer range – required for the destruction of the cloud system and the formation of precipitation. Therefore, from our point of view, it is optimal to inject pre-prepared powders when the goal is to increase precipitation.

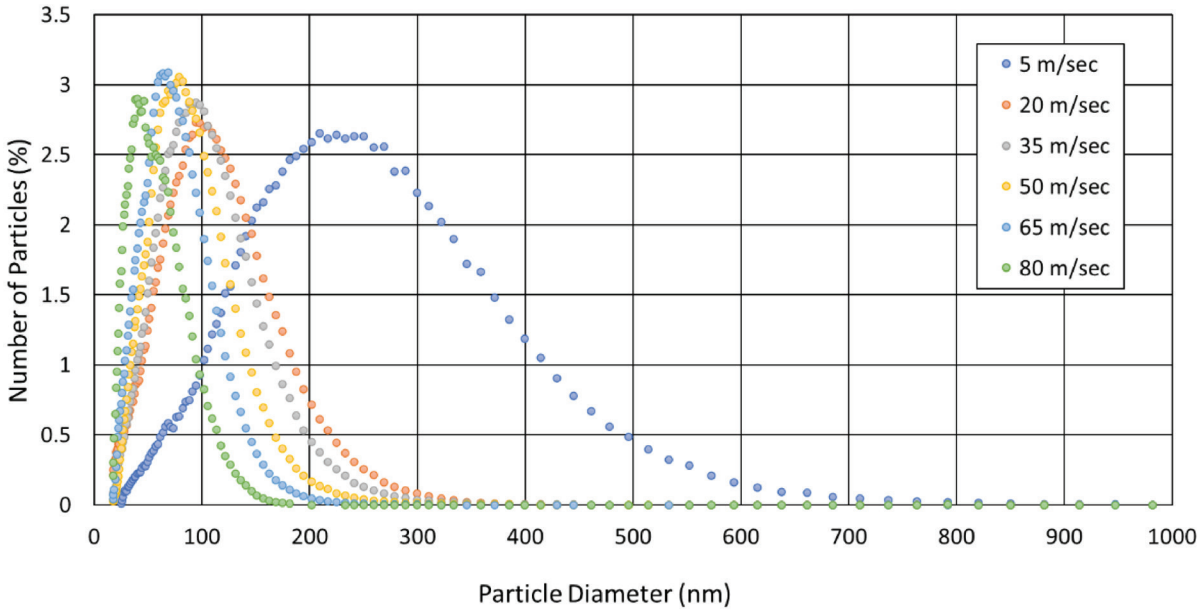

Fig. 4. Change in the spectrum of hygroscopic aerosol formed during the combustion of a torch with the composition 1 at air speeds from 5 to 80 m/s.

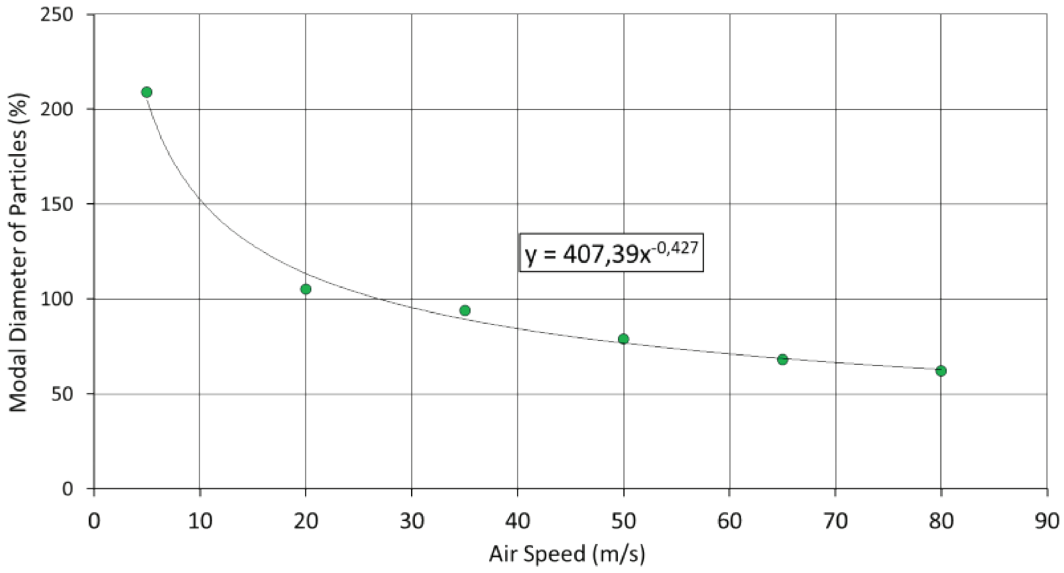

Fig. 5. Change in the modal diameter of the hygroscopic aerosol composition 1 as a function of air speeds from 5 to 80 m/s.

2.4 Insertion of hygroscopic powder-like aerosols to the cloud environment.

An alternative to the use of hygroscopic aerosols generated by pyrotechnic compositions is the use of pre-prepared powders. The advantage of this method is the constancy of the composition of the powder, as well as the spectrum of the aerosol when using specific dispersion systems, regardless of the speed and flight altitude of the aircraft.

It should also be noted the problems that arise when using this technology:

1. Since micrometer-sized particles have a high tendency to adhere, anti-caking agents must be added to the powder. Since this additive is characterized by nanometer size ranges, the manifestation of hygroscopic properties by the particles of the additive can lead to a tendency to stabilize the colloidal medium.

2. When studying the spectrum of an aerosol of a pre-prepared powder, it is very problematic to justify which particles are present in the nanometer part of the spectrum - whether they have hygroscopic properties or not. The only practical way to obtain such information is to directly conduct an experiment in a cloud chamber with a study of the dynamics of the spectrum of droplets of a colloidal system.

3.0 RESULTS AND DISCUSSION

3.1 Comparative impact of hygroscopic aerosol of various origins on the cloud environment.

Cumulus Cloud Modeling Environment.

The cloudy environment formed due to adiabatic cooling, with initial relative humidity of 90%, the temperature at 295 K, the rate of adiabatic cooling is equivalent to the rate of rise of the air mass at a speed of 2 m/s. The experiment is described in more detail by A. S. Drofa, V. N. Ivanov, D. Rosenfeld, and A. G. Shilin in Studying an effect of salt powder seeding used for precipitation enhancement from convective clouds, 2010.

The dynamics of changes in the cloudy environment in the climatic chamber under background conditions and in the case of the introduction of aerosols with the spectra presented above is shown in Figure 6.

If in the background experiment when simulating the implementation of a convective cloud process under conditions of experience, the number of

initially formed droplets slightly exceeds 1000 drops per cubic centimeter, under the same conditions for the formation of a cloud medium, in the case of the presence of an aerosol formed during the combustion of a pyrotechnic composition, the number of drops exceeds ten thousand, and in the case of pre-introduced aerosol of micrometer size is at the level of several hundred. In the case of an aerosol in the nanometer range, the situation is even more pronounced than what is shown in the chart, since both the number of particles and the amount of mist droplets will peak at the lower detection limit of the instruments used.

This is reflected both in the amount of precipitated water (Figure 7), and in the lifetime of the colloidal system.

If the lifetime of the latter in a cloud chamber under background conditions is in the range of 30-40 minutes, in the case of the presence of a nano dispersed hygroscopic aerosol, the cloud system exists up to several hours, and in the case of the aerosol of micrometer sizes, the lifetime is reduced to 15-20 minutes.

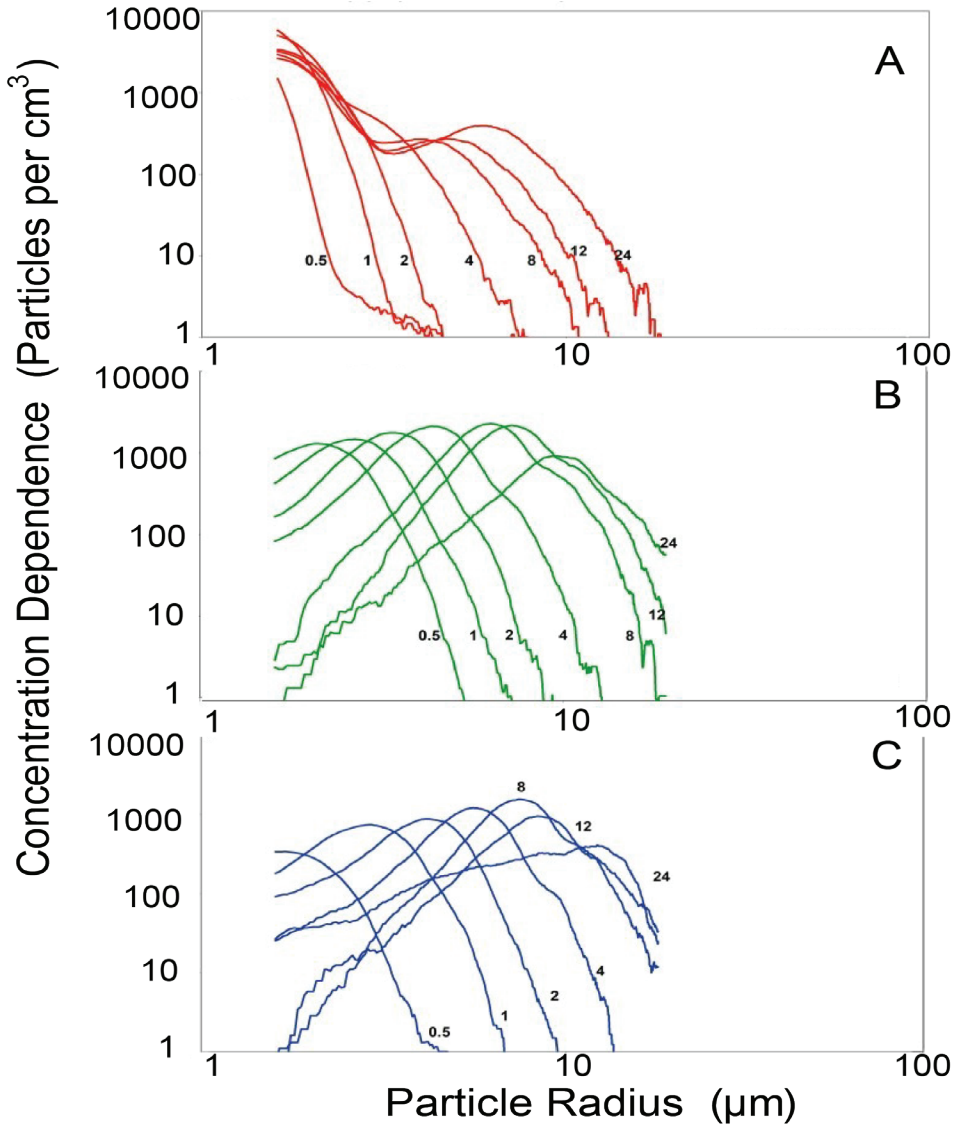

Fig. 6. The observed evolution of cloud drop spectrum in the cloud chamber measured at times noted from 0.5 to 24 minutes from the moment of formation of the cloudy environment.–Chart A is the Pyrotechnic composition - B is the background experiment, and Chart C shows the results in the presence of pre-prepared powder.

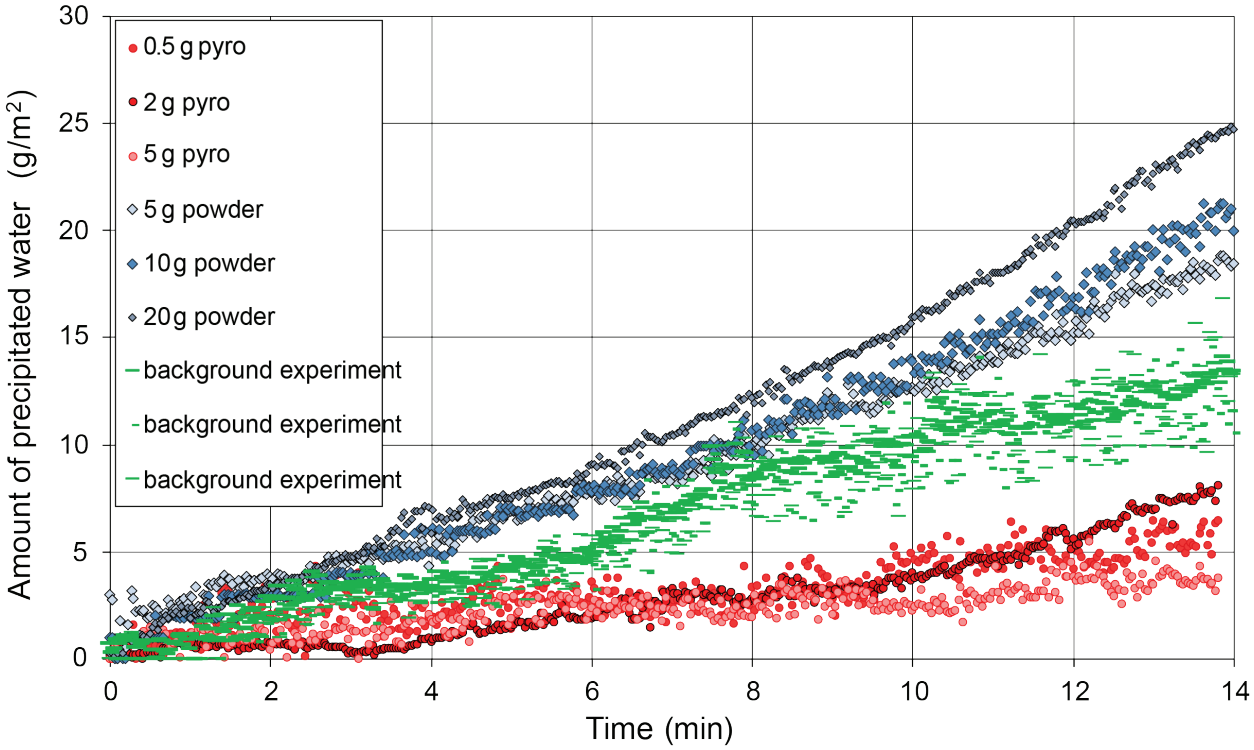

Fig. 7. The amount of water deposited over time on a test site. Accordingly, 5, 10, 20 g of powder was introduced into the chamber and burned 0.5, 2 and 5 grams of pyrotechnics, (a higher position of the dependence corresponds to a larger amount of powder introduced).

Our research suggests that artificial aerosol particles in the first case (Figure 6, A), with more pronounced hygroscopic properties in the process of adiabatic cooling and the associated increase in relative humidity turn out to be in more favorable conditions. Under these conditions, natural CCN either does not appear or their participation in the process is negligible and the process is driven by the presence of a large amount of aerosol of pyrotechnic origin.

In the third case (Figure 6, C), the main amount of water vapor is intercepted by artificial nuclei and natural nuclei do not participate in the process of water vapor absorption or their contribution to this process is very small.

We emphasize that in the first case the colloidal system is more stable. Aerosol nanoparticles, due to their chemical properties (meaning the formation of compounds of the $xMeCl_y * zH_2O$ type) and hygroscopicity, inevitably absorb water vapor, increasing in size. But a result of the development of the condensation process creates a more dilute solution (decreasing effect of Raoult's law in combination with an increase in vapor pressure caused by a significant curvature of the droplet surface) further preferential droplet growth becomes impossible. The reverse process - the drying of drops - is also impossible because this increases the concentration of the solute. The result is a colloidal system capable of long-term existence.

3.2 Impacts on the nimbostratus cloud modeling environment.

Simulation Conditions: The predominant droplet size is from 7 to 8 microns with fluctuations from 2 to 72 microns, Droplet concentration from 100 to 1000 cm^3.

The impact of hygroscopic aerosols of various size ranges is qualitatively similar to the cumulus cloud simulation process; however, due to the small size

of the droplets, the dynamics of the experiment are somewhat different (Figure 8).

3.3 Impacts on the environment simulating stratus clouds.

Simulation parameters: dominant droplet size from 4 to 7 μm, Droplet concentration from 100 to 1000 cm^3.

Due to the small diameter of cloud droplets and low water content in the case of stratus clouds, it is difficult to increase the amount of precipitation when exposed to powders, however, the effect of an aerosol of a nanometer size range stabilizes the cloud to a large extent (Figure 9). This is reflected not so much in the decrease in the amount of water deposited from the layered cloud system, an amount that is already miniscule, but in the duration of its existence in the chamber. While under background conditions, the existence of a stratus cloud in the chamber can be maintained for no more than 40 minutes, if enough hygroscopic aerosol of pyrotechnic origin is introduced, the cloud can exist for several hours or more.

The information obtained allows us to formulate the following provisions:

1. Exposure to an aerosol of nanometer size range (of pyrotechnical origin) stabilizes the cloud to some extent in the case of any model media.

2. The stabilization process is the more pronounced, the more pyrotechnic aerosol is introduced into the cloudy environment and the more the aerosol spectrum is shifted towards smaller sizes.

3. Aerosol exposure to pre-formed powder either results in increased precipitation in cumulus and nimbostratus cloud, or in the case of stratus cloud simulation exposure causes no significant change, but in no case results in stabilization of the cloud environment.

4. In all cases of exposure to aerosol in the micrometer size range, the statement “a larger amount of aerosol leads to an increase in precipitation” is true to one degree or another.

5. In all cases of exposure to aerosol in the sub micrometer size range, the statement “a larger amount of aerosol leads to a decrease in precipitation” is true to one degree or another.

3.4 Ways to increase the efficiency of hygroscopic aerosol generators.

It is possible to vary the distribution of particles formed in the process of thermal condensation either by changing the composition of the pyrotechnic mixture or the design of the generator, or by changing the speed of air in the condensation zone. In this case, the following regularities should be noted:

1. The change in air speed makes the biggest contribution to the change in the aerosol spectrum. The greater the air speed, the more the spectrum of the formed aerosol shifts towards smaller particle sizes.

2. Generator design: the larger the area of the burning surface and speed of production of the aerosol-forming material, the more the aerosol spectrum shifts towards larger sizes.

3. The composition of the pyrotechnic mixture: In general, there is a very small relationship between the parameters of the pyrotechnic mixture (combustion temperature, condensation temperatures of high-boiling components, the volume of gases released during combustion) and the spectrum of the formed aerosol, however, the presence of high-boiling components in the combustion products most likely contributes to the enlargement of the spectrum of the formed aerosol.

Hence, to increase precipitation, since the implementation of the colloidal instability of a cloudy medium is possible only when particles or drops appear that are significantly larger than the average size of the ensemble, it is preferable to use pre-prepared powders. The use of pyrotechnic generators

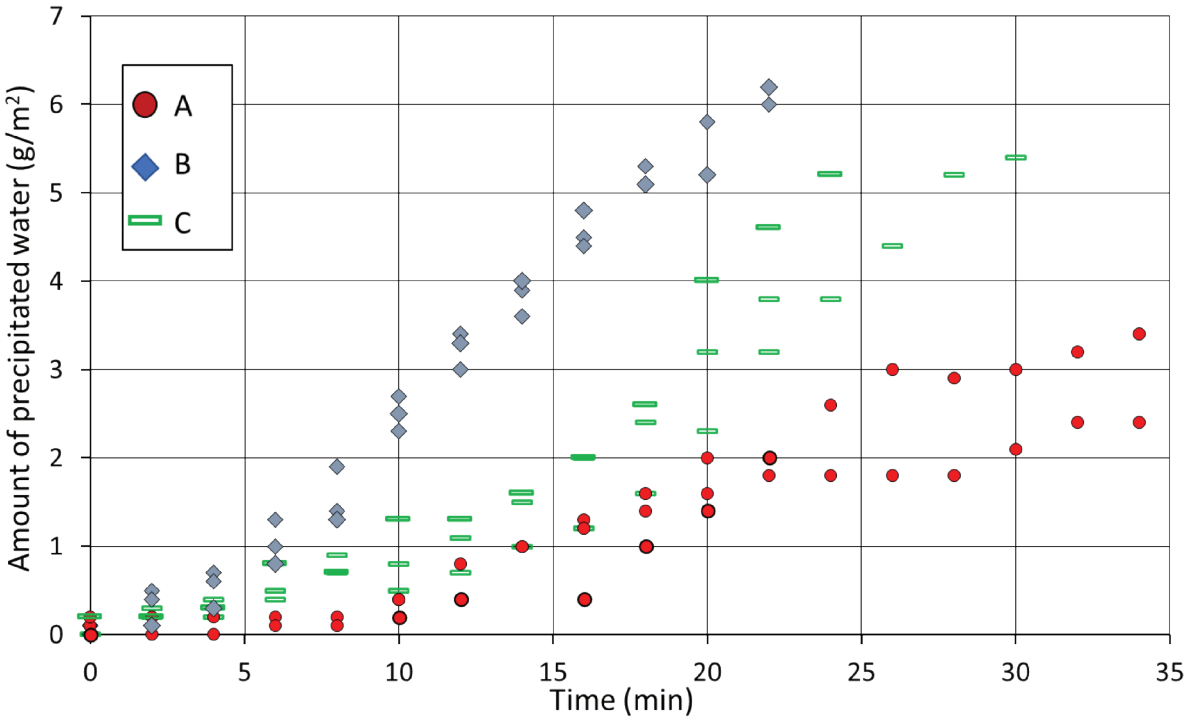

Fig. 8. The amount of water deposited over time on a test site. Marker A - background experiments. Marker B - exposure to various concentrations of hygroscopic aerosol from a pyrotechnic generator (higher aerosol concentrations correspond to a lower location of points). Marker C - exposure to an aerosol of pre-prepared powder. Accordingly, 5, 10 g of powder was introduced into the chamber, a higher position of the dependence corresponds to a larger amount of powder introduced.

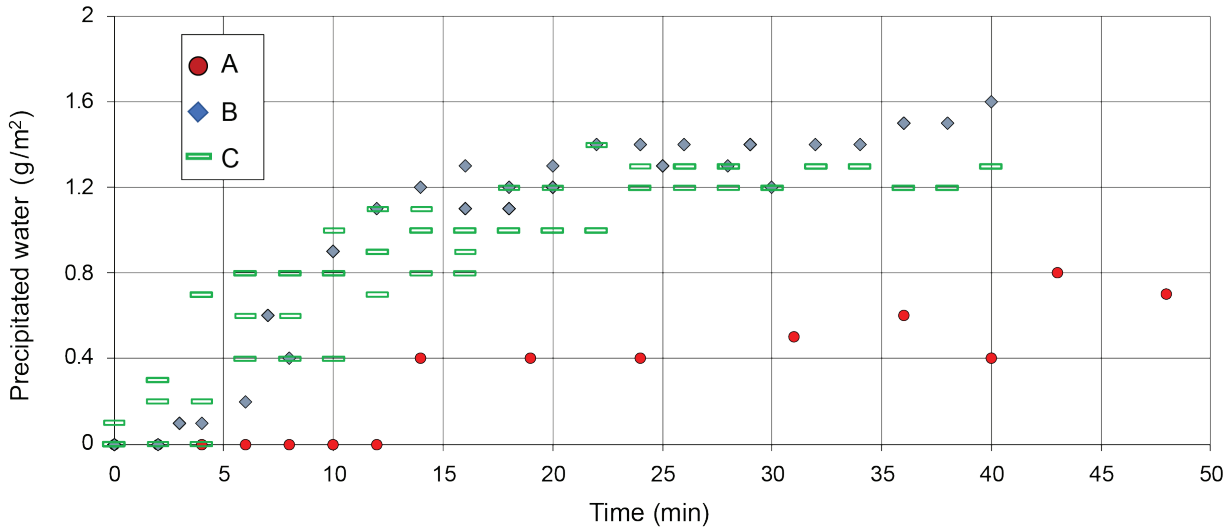

Fig. 9. The amount of water deposited over time on a test site. Marker A - background experiments. Marker B - exposure to hygroscopic aerosol of a pyrotechnic generator. Marker C - exposure to an aerosol of pre-prepared powder. Accordingly, 5, 10, 20 g of powder were introduced into the chamber.

makes sense only in situations where there is little or no air movement at the generator (wind speeds less than 5 m/s). As in the previous case, when studying the effect of powders, we did not find the effects of reseeding - that is, in general application, an overdose of the powder has no adverse effects.

4.0 CONCLUSIONS

It has been confirmed experimentally that it is impossible to obtain an aerosol in the micrometer size range by thermal condensation methods in the conditions associated with the actual use of the generator from the aircraft. This makes it possible to critically evaluate the results of work on increasing precipitation using hygroscopic pyrotechnic torches (Hygroscopic Burn-In-Place Flares). Experts within the World Meteorological Organization (WMO) are now beginning to come to the same conclusion (WMO 2018).

The factors that determine the spectrum of aerosols obtained by thermal condensation have been studied. It is shown that the compositions of the same class with respect to the content of the condensed phase in the combustion products form aerosols of approximately the same spectrum, which changes very slightly depending on the combustion temperature. The area of the burning composition has a greater influence on the aerosol spectrum, but the air speed around generator has the greatest influence.

The insertion of hygroscopic aerosols in the 1-10 micrometer size ranges can yield an increase in precipitation efficiency in modeled clouds - cumulus, stratocumulus, and stratus. Depending on the type of cloud environment, the efficiency can be significant (maximum for cumulus clouds and minimum for stratus clouds) but in no case was there a change in trend (decrease in the amount of deposited water compared to the natural process).

Future work is recommended to further understand the processes underlying the laboratory-based results pertaining to using powder reagent-coated aerosols as warm cloud seeding agents.

5.0 REFERENCES

Drofa, A. S., V. N. Ivanov, D. Rosenfeld, and A. G. Shilin, 2010: Studying an effect of salt powder seeding used for precipitation enhancement from convective clouds. *Atmos*. *Chem*. *Phys*., **10**, 8011–8023, https://doi.org/10.5194/acp-10-8011-2010.

Bruintjes, R. T., Salazar, V., Semeniuk, T. A., Buseck, P., Breed, D. W., & Gunkelman, J., 2012: Evaluation of Hygroscopic Cloud Seeding Flares. *The Journal of Weather Modification*, 44(1), 69–94. https://doi.org/10.54782/jwm.v44i1.85

Cooper, W. A., R. T. Bruintjes, and G. K. Mather, 1997: Calculations Pertaining to Hygroscopic Seeding with Flares. *J*. *Appl*. *Meteor*., **36**, 1449–1469, https://doi.org/10.1175/1520-0450(1997)036<1449:CPTHSW>2.0.CO;2.

DeFelice, T. P., J. Golden, D. Griffith, W. Woodley, D. Rosenfeld, D. Breed, M. Solak, and B. Boe, 2014: Extra area effects of cloud seeding — An updated assessment. *Atmospheric Research*, **135–136**, 193–203, https://doi.org/10.1016/j.atmosres.2013.08.014.

Hamer, W. J., and Y.-C. Wu, 1972: Osmotic Coefficients and Mean Activity Coefficients of Uni-univalent Electrolytes in Water at 25°C. *Journal of Physical and Chemical Reference Data*, **1**, 1047–1100, https://doi.org/10.1063/1.3253108.

Haryanto U., Goenawan R. D., Harsanti D. The Development of Hygroscopic Cloud Seeding Flare In Indonesia: Evaluation and Measurement of Distribution Particles, Badan Pengkajian dan Penerapan Teknologi (BPPT), 2011.

Mather G.K. Method of cloud seeding, patent US 5357865, https://patents.google.com/patent/US5357865A/en, Water Research Commission, 1994.

Murakami M. and JCSEPA research group. Japanese Cloud Seeding Experiments for Precipitation Augmentation (JCSEPA), 2006 – 2011.

Rosenfeld, D., D. Axisa, W. L. Woodley, and R. Lahav, 2010: A Quest for Effective Hygroscopic Cloud Seeding. *Journal of Applied Meteorology and Climatology*, **49**, 1548–1562, https://doi.org/10.1175/2010JAMC2307.1.

Rosenfeld D., Woodley W. L. New insights and methodologies for the operational assessment of seeding potential. WMA, Las Vegas, NV, April 27, 2012.

Segal, Y., A. Khain, M. Pinsky, and D. Rosenfeld, 2004: Effects of hygroscopic seeding on raindrop formation as seen from simulations using a 2000-bin spectral cloud parcel model. *Atmospheric Research*, **71**, 3–34, https://doi.org/10.1016/j.atmosres.2004.03.003.

Segal, Y., M. Pinsky, and A. Khain, 2007: The role of competition effect in the raindrop formation. *Atmospheric Research*, **83**, 106–118, https://doi.org/10.1016/j.atmosres.2006.03.007.

Wang, F., Z. Li, Q. Jiang, G. Wang, S. Jia, J. Duan, and Y. Zhou, 2019: Evaluation of hygroscopic cloud seeding in liquid-water clouds: a feasibility study. *Atmos*. *Chem*. *Phys*., **19**, 14967–14977, https://doi.org/10.5194/acp-19-14967-2019.

Su Z. Weather Modification Centre of China Meteorological Administration (WMC, CMA), Joint RFBR-NSFS seminar, Beijing, 16-21 April 2019.

WF-1 Airborne Pyrotechnic Flare Seeding System. China Meteorological Administration, 2010.

Zou L., Jouiad M., Zaki A., Hadri E.N., Liang H. Using Nanotechnology to develop novel cloud seeding materials for Rain Enhancement. Masdar Institute of Science and Technology. The First International Research Progress Workshop. UAE 18-19 January 2017.

WARM FOG ELIMINATION BY SEEDING WITH SALTY DROPS: EXPERIMENTS AND THEORY

Alexander Khain[1], Mark Pinsky[1], Ehud Gavze[1], Ayala Ronen[2],
Shmuel Elisha[2], Ofir Shoshanim[2] , and Pavel Khain[3]

[1]*Institute of Earth Science, The Hebrew University of Jerusalem, Jerusalem, Israel*
[2] *Department of Environmental Physics, the Israel Institute for Biological Research, Ness Ziona, Israel*
[3]*Israel Meteorological Service, Bet Dagan, Israel*

ABSTRACT

A method for warm fog elimination by seeding with salty drops was tested in a fog chamber in laboratory experiments, a field experiment, and by a geometrically simple numerical model with an accurate calculation of condensational growth and evaporation of fog droplets and seeding salty drops. The laboratory experiments, conducted in a 3 × 3 × 2.7 m fog chamber, showed an increase in visibility from a few meters to about 100 m in several seconds after seeding. A field experiment in which natural fog was seeded with salty drops ejected for 10 s over an area of 6 × 6 m from heights of 3 and 10 m showed a substantial increase in visibility for about 1.5-2 min. The limited duration of increased visibility was related to the background wind that advected the environmental fog into the seeded area. The numerical model successfully reproduced the laboratory and field experiments' results. The numerical model was used to analyze optimal seeding regimens and visibility sensitivity to the concentration, size, and salinity of the seeding drops, concentration of the fog droplets, the height of seeding, and other parameters.

1.0 INTRODUCTION

Fog decreases visibility and, consequently, creates a serious problem for the transportation and aviation systems in many countries. Airports stop working when visibility is lower than 500 m. Fog leads to considerable losses in other areas, such as at ski resorts. Therefore, fog elimination is one of the main weather modification activities that have attracted researchers' attention for many years.

There are two fog types: mixed-phase fog (at sub-zero temperatures), consisting of ice particles and liquid droplets, and warm fog, consisting of small liquid droplets and haze particles. The main approach to eliminating mixed-phase fog is seeding it with ice formation agents like "dry ice" (solid CO_2) or submicron AgI particles that, being efficient ice nuclei, produce ice particles at temperatures around –5 ºC. The goal of such seeding is to increase the concentration of ice particles that intensify the Weber-Bergeron-Findailsen mechanism and lead to ice particle growth at the expense of liquid droplet evaporation. Large ice particles are expected to sediment, thereby increasing visibility.

Elimination of warm fog represents an especially difficult problem. The low visibility in the fogs is caused by a high concentration of small droplets with a radius of 1 μm to 5 μm. Since very small droplets do not collide or sediment, the fog droplets remain in the air for a long time, till the air temperature increases and humidity decreases. Several approaches have been proposed to eliminate warm fog (Frost et al. 1980). The first approach was heating the air to lead the fog droplets to evaporate. Some airports used sets of turbo-reactive engines; however, this method is energy-expensive when large air volumes should be heated. Besides, using this method in airports might be inconvenient and even dangerous (Frost et al. 1980).

Another approach to evaporate the fog is by creating downdrafts with helicopters. Fog evaporation is caused by mechanically mixing the fog and the warm, dry air above it. The potential temperature increases and humidity decreases with height, so the mixing leads to fog heating and dilution. According to Frost et al. (1980), the mixing is inefficient, helicopters can clear the fog for only short durations, and their presence over runways can affect regular airport traffic.

Another idea to eliminate warm fog is to charge some of the fog droplets. It is possible to charge some droplets with a positive charge and others with a negative charge. Khain et al. (2004) (see also European Patent EP1467611B1) showed that seeding fog with charged drops increases the collision rate between them and the fog droplets, fostering settling of the latter. This process leads to a decrease in the fog droplet concentration and an increase in visibility. The drawback of this and other methods of charging the fog droplets (for instance, by moving the fog droplets through a filter or electrostatic mesh with high electric potential) (e.g., Chernikov and Khainkine 1999) is the need for a high-power generator to produce charged droplets for seeding large fog volumes, or the utilization of high-voltage equipment to charge fog droplets. Only a small distance of fog is eliminated when using a metallic mesh.

Beginning with the study by Houghton and Radford (1938), fog seeding with dry hygroscopic nuclei has been considered the most prospective and efficient method to eliminate warm fog. The hygroscopic seeding with flares containing hygroscopic salts (NaCl, $CaCl_2$, KCl, etc.) of clouds and fogs have been tested since the 1990 (Mather et al. 1997). In the case of cloud seeding the goal as to accelerate (trigger) precipitation formation. Droplets formed on the hygroscopic particles grow faster than other cloud droplets and play the role of collectors colliding other cloud droplets. Segal et al. (2004) showed that the optimum radius of hygroscopic particles to seed clouds is about 2 micron. The droplets forming on these particles in the conditions of cloud supersaturation rapidly reach the sizes of about 16-18 micron allowing collect smaller droplets.

The hygroscopic seeding of warm fog does not aim formation of precipitation. In contrast, the goal of the seeding is to evaporate small fog droplets. Indeed, dry hygroscopic nuclei grow by absorbing water vapor at relative humidity (RH) of < 100%. For example, dry particles of NaCl start growing when the RH exceeds the deliquesce humidity, which is about 75%. Water vapor absorption by hygroscopic nuclei decreases RH of the air below 100%, leading to fog droplets evaporation and increased visibility. Several numerical models of seeding warm fog with dry hygroscopic nuclei have been developed to justify this method (Jiusto et al. 1968; Kornfeld 1970; Koenig 1971; Kunkel and Silverman 1970; Silverman and Weinstein 1973; Silverman 1973). For instance, Kunkel and Silverman (1970) simulated fog seeding with monodispersed salt particles (NaCl) using a 1D fog model. They found that the optimum radius of salt particles was 5 μm, when fog dissipation lasted for a few minutes. Zhao (1989) conducted a numerical simulation of warm fog dissipation with a two-dimensional fog model coupled with the growth equation of hygroscopic particles. Using a one-dimensional fog model, Huang (1988) studied warm fog dissipation by salt particle seeding and concluded that the effect of fog dissipation by 20–30 μm in the diameter salt particles with a seeding particle mass of 0.54–0.91 gm^{-3} was most notable. One of the most recent papers dedicated to this problem is the study by He et al. (2016) in which the dissipation of a warm fog event during 6–7 November 2009 in the Beijing and Tianjin area was simulated by implementing a salt-seeding and 2-moment explicit cloud schemes in the Weather Research Forecasting system (WRF). They simulated seeding with 80 μm dry particles. Reuge et al. (2017) used fog 1-D model to simulate fog removal by seeding with salt particles of ~3-4 μm in radius and three chemical compositions: NaCl, $CaCl_2$, and KCl. They concluded that seeding with NaCl particles was the most efficient. According to the evaluations by Reuge et al. (2017), seeding of

~15 kg of such particles can eliminate fog within the volume 0.25 km^2 x 40 m during 17 min.

Since an accurate simulation of the growth of initially dry particles requires extremely small time steps, the description of chemical processes in the models included many simplifications and limiting parameters (e.g., the deliquescence step is ignored, fog is considered as pure water droplets, Reuge et al. 2017). Typically, the initial stage of and particle growth is not analyzed. At the second stage, when the particles became large, and the absorbed water mass became much larger than the initial dry seed particles' mass, the models showed an increase in visibility. Their results showed that it was possible to dissipate warm fog locally with salt particles and that larger salt particles and seeding amounts improved the seeding effect. The background wind effects were not considered.

A primary goal of the numerical studies was to determine the optimal hygroscopic seed particle size. Very small seed particles (1–10 μm) fall slowly, forming new fog particles that decrease visibility. Very large particles fall too fast, so the fog evaporates only partially. Furthermore, seeding by very large particles requires a large mass of salt, which is inefficient and induces ecological problems.

Fog seeding with dry hygroscopic particles was performed at the Cornell Aeronautical Laboratory in a 600 m^3 fog chamber (Jiusto et al. 1968; Koenig 1971) and in several airborne seeding experiments using a DC-3 aircraft and a helicopter to dispense the hygroscopic material at the fog top. An extensive battery of ground instrumentation recorded the seeding effects on visibility. Results of the Noyo Valley experiments led to the establishment of a semi-operational test program at McClellan Air Force Base in Sacramento, California, in January 1971. A C-130 aircraft and an Air Force helicopter were used as the seeding vehicles during tests in 1968–1969 (Silverman and Smith 1971).

Although a significant part of the experiments showed increased visibility, the approach was not widely utilized. Planes were used to carry out the hygroscopic seeding of clouds and fogs. Nowadays, drones can be used which have to decrease the costs of this technique (Pyper Vision 2022).

The hygroscopic particles tended to grow in humid air and created conglomerates. Hence, it was extremely difficult to control the hygroscopic particle size being seeded. Conglomeration led to a wide size distribution of the seeding particles that differed from the initial distribution and was not optimal. Small hygroscopic particles grew slowly in the fog and did not sediment or sedimented slowly. Consequently, these particles formed an additional, artificial salty fog that decreased the visibility rather than increasing it. Note that in some numerical studies visibility of fog only was evaluated, without considering the contribution of seeding drops (e.g., Reuge et al. 2017). Very large particles could help to increase visibility, but they fell rapidly. Moreover, choosing the optimal seed particle size was impossible as it depended on various conditions such as the fog layer depth and density, wind speed, and more. Utilization of non-optimal seed particle size could lead to weak and ineffective seeding. Besides, the cost of producing carefully-sized materials was very high (Frost et al. 1980).

Below, we describe laboratory and field experiments and a numerical simulations of fog elimination by seeding it with liquid drops containing surfactants (NaCl or $MgCl_2$). Such seeding with drops can be performed by simple sprinklers. The physical principle of the method is similar to that of seeding with hygroscopic particles. Salty drops grow at RH < 100%, dry the air, and lead to fog evaporation. The advantage of this method is the possibility to control the seeding drop size to make them close to the optimal size. The lack of conglomeration and the possibility to change the seeding drop size based on microphysical parameters of the fog, are important advantages of the proposed approach. Following is the structure of this paper. In Section 2, we discuss the results of laboratory and field experiments. In Section 3, we present the

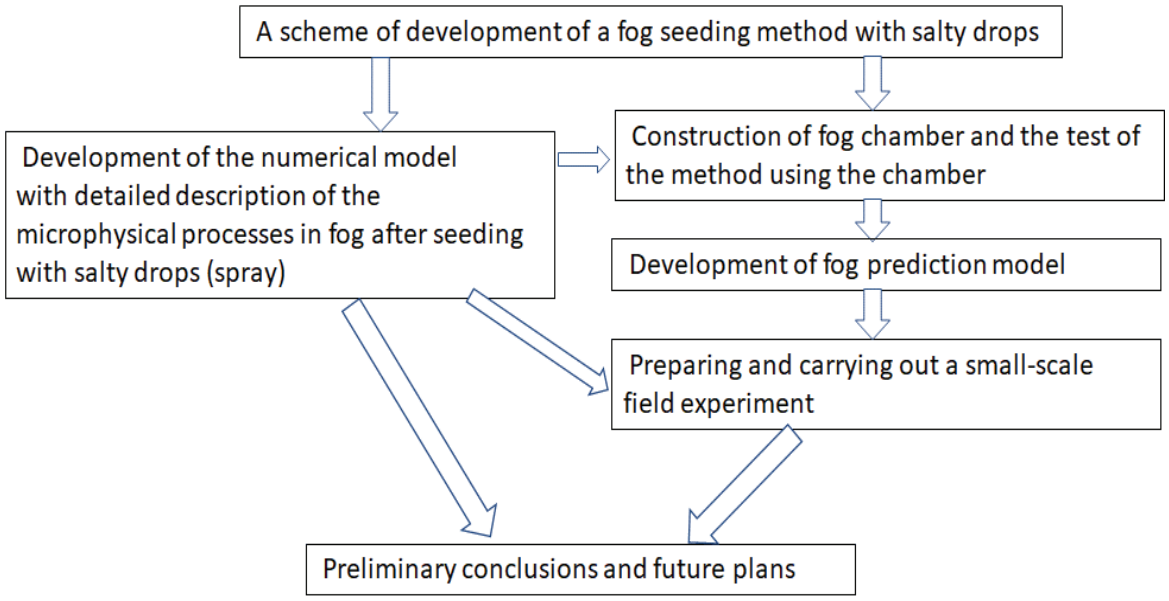

Fig. 1. A scheme of the method development and testing.

results of fog seeding modeling. Section 4 presents our conclusions. A scheme of the present study reflecting the milestones is presented in Fig 1.

2.0 EXPERIMENTAL TEST OF THE METHOD

2.1 Experiments in a Fog Chamber

Description of the fog chamber. We designed and constructed a fog chamber at the Israel Institute for Biological Research to verify the concept of fog elimination by seeding it with salty drops. The fog chamber size was 3 × 3 × 2.75 m. The scheme of the fog chamber is shown in Fig. 2. The chamber was filled with fog produced by several ultrasonic aerosol generators characterized with size distribution centered at a radius of 4–5 μm, within the range of natural fog radii (Frost et al. 1980). The seeding sprinklers were placed near the ceiling. Visibility was measured by three laser-photo diode systems positioned at three heights: 1, 1.5, and 2 m. Measurements of the temperature, RH, visibility, and droplet size distribution functions were visualized on computer screens online. An image of the fog chamber is shown in Fig. 3a. Fig. 3b shows the set of sprinklers placed near the ceiling. The sprinklers produce drops with a diameter distribution range between 50 and 200 μm, depending on the air and water pressures in the sprinklers. The instantaneous sizes of seeding drops (hereafter, spray) as well as fog were measured in the course of experiment using the laser diffraction system, "Spraytec" [Malvern].

The visibility inside the chamber was monitored by measuring the transmittance across the chamber at three different lines of sight by self-built optical transmissometers, each of them consists of a laser diode (ThorLabs) at a wavelength of 638.3 nm and two photo-detector channels for the transmitted signal and the clear reference.

Results of the laboratory experiments. Three groups of fog seeding experiments were performed in the fog chamber. In the first group of experiments, the chamber was filled with fog, and the RH was established at about 100%. Initial visibility was only 2.7 m, i.e., fog was very dense with high liquid water content (LWC) of about 0.5–1.0 gm^{-3}.

a. No seeding was performed in the first group of experiments. The goal was to check the stability of the fog and attribute the increase in visibility to the seeding only. The results showed that the fog remained stable and

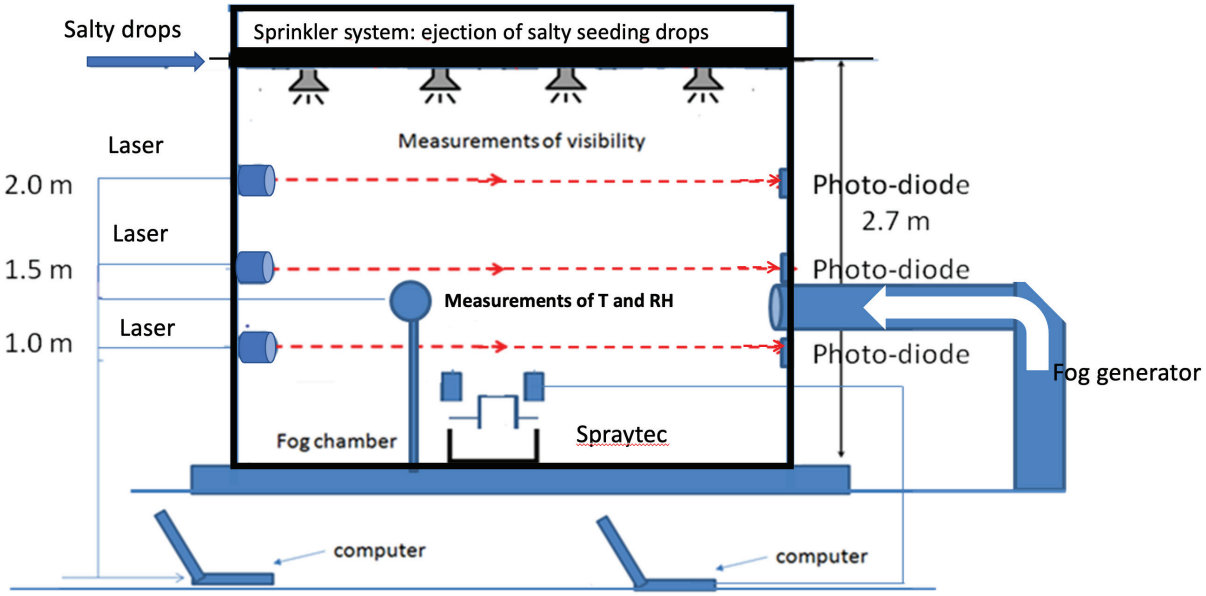

Fig. 2. A scheme of the fog chamber.

Fig. 3. Left: A photo of the fog chamber. Right: The set of sprinklers constructed near the fog chamber's ceiling.

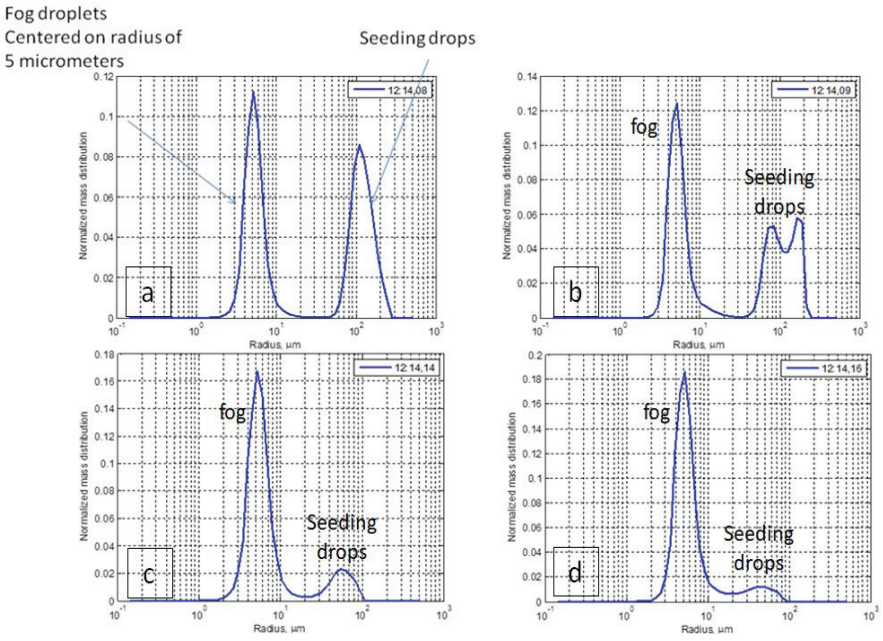

Fig. 4. Size distributions of fog droplets and freshwater seeding drops at various time points as measured with the Spraytec. Numbers denote time: h, min, s. The time difference between panels (d) and (a) is 8 s.

visibility remained unchanged for at least 15 min (Fig. 5a). This stability was reached by thermally isolating the fog chamber walls. The thermally-isolated chamber maintained a stable temperature for a long time, keeping the RH at the equilibrium state. The fog stability suggests that coagulation and sedimentation processes are negligible. Since artificial fog droplets are salinity-free, the equilibrium saturation should be very close to 100%.

b. In the second group of experiments, the fog was seeded with freshwater (non-salty) drops of the same size distribution as that used later for seeding with salty drops. These experiments aimed to evaluate the effect of collisions between the seeding drops and the fog droplets on visibility and to stress the importance of including salt in the drops. The results of these experiments showed that non-salty drops did not affect the fog and its visibility. The results of the first and second experiment groups were very similar. The fog droplet and seeding drop size distributions at various time points measured during a second-group experiment are shown in Fig. 4 and 5a. The smaller droplets' peak, centered at around 5 μm, represents the fog droplets, and the larger drop peak represents the seeding drops (spray) that had a maximum drop radius of 100 μm. In this experiment, freshwater spray did not affect fog distribution and visibility. The amplitude of the spray mode decreased with time due to sedimentation. The largest spray drops fell first, leading to a shift of the spary size distribution peak toward smaller drop sizes. The amplitude of the fog mode did not change, suggesting that collisions between the seeding drops and fog droplets were negligible, even at such a high fog concentration. The freshwater seeding drops did not affect the fog, so they could not increase visibility. The negligible effect of spary-fog droplets collisions was reported also by Reuge et al. (2017). Indeed spray drop with the radius of 100 μm falling with the velocity of 100 cm s^{-1} from height of 3 m will collect about 20 fog droplets of the 5 μm radius and fog concentration of 500 cm^{-3} (the collision efficiency between 100 μm

and 5 μm radii drops is about 0.5, Khain and Pinsky, 2018). At the same time concentration of fog is about 10^3–10^4 larger than that of spray. As a result, spray can decrease fog concentration not more than a few percent.

c. The fog was seeded with salty drops in the third group of experiments. These experiments showed a dramatic increase in visibility. Through this set of experiments, we changed the seeding drop salinity, chemical composition, and size, and the initial fog visibility. We present several typical examples of the results.

Fig. 5a shows the time dependencies of visibility in a laboratory experiment in which the fog was seeded by NaCl drops with an initial salinity of 23% (salinity was calculated as the ratio between the salt mass in a drop and the drop mass). The salinity was close to the maximum for NaCl. The initial fog visibility was 2.7 m, and the seeding duration was 1 s. The time dependencies of visibility in the fog-only (red dotted line) and freshwater drop seeding (blue dotted line) experiments are presented for comparison. As mentioned above, visibility in the fog-only freshwater drop seeding experiments did not change significantly through the experiment durations (10 min). Conversely, seeding with salty drops led to a 15–25 times increase in visibility during several minutes.

One can see that the time dependencies of visibility consisted of two segments with different slopes. The first segment showed a fast (within ~10 s) increase in the visibility, followed by continuous slow growth in the visibility. The fog evaporates during the first, short segment, leading to a fast increase in the visibility. The slower increase in the visibility during the second segment was related to a decrease in the spray concentration due to the sedimentation of the smallest spray. The spray first went past the z = 2 m level. As a result, the fast growth in visibility at this level was replaced by slower growth in visibility.

Since the vertical distance between larger and smaller spray drops increased with time due to differences in their fall velocities, the seeding drops

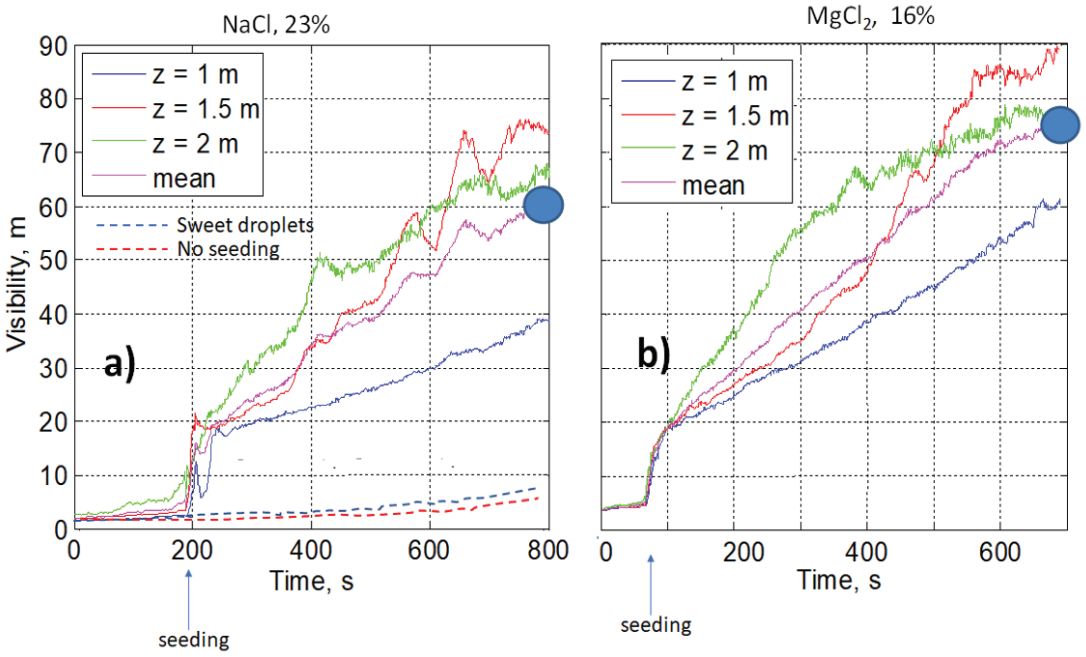

Fig. 5. Time dependencies of visibility in the fog chamber during several laboratory experiments: a) seeding with NaCl solution drops; b) seeding with $MgCl_2$ solution drops. The seeding duration was 1 s, and the mass of seeded water drops was 90 g. The red dotted line in panel (a) denotes "Fog only" (no seeding), and the blue dotted line denotes seeding with freshwater drops. Visibility at three heights of photo-diodes and the mean visibility are shown.

took the longest to pass through the z = 1 m level.

An interesting visibility behavior at the z = 1 m level was seen at t = 220 s (Fig. 5a) when a short-term decrease in visibility was measured. We attribute this short drop in visibility to a temporary high spary concentration.

The effect of the spary' chemical composition is illustrated in Fig. 5b. One can see that $MgCl_2$ spray increased the rate of visibility increase even when the solution was less concentrated than in the case of NaCl. As $MgCl_2$ has a higher hygroscopicity than NaCl, it decreases the RH more than NaCl.

An important practical question is the sensitivity of visibility to the spray' mass. Fig. 6 compares the time dependencies of visibility in experiments with seeding drops ($MgCl_2$) at seeding durations of 1 s (a) and 0.5 s (b). The total spray masses were 70 and 32 g, respectively. Interestingly, the visibility reached a higher value when seeding duration was 0.5 s. This result indicated the existence of an optimal seeding drop mass. The spray mass should be high enough to evaporate the fog; however, an increase in the mass beyond the optimum decreases visibility because the spray also affects visibility.

Other experiments indicated that a lower seeding drop mass was required at higher initial visibility. Seeding in short pulses was more efficient than continuous seeding.

2.2 Field Experiment

The differences in conditions between laboratory and field experiments are significant. First, natural fog droplets form on soluble aerosols and represent a very diluted solution. Second, the wind in the atmosphere is non-zero, and the atmosphere is turbulent. As a result, the seeded air volume moves downwind from the seeding place and mixes with the surrounding air. Therefore, eliminate fog under natural conditions is more difficult than in a closed fog chamber in which spatial boundaries are well defined. The main goal of the field experiment was to confirm our hypothesis that natural fog seeding with salty drops could increase visibility.

Design of the field experiment. The field experiment scheme is shown in Fig. 7. The sprinkler matrix size was 6 × 6 m, and the distance between sprinklers was 1.0 m. The sprinklers were

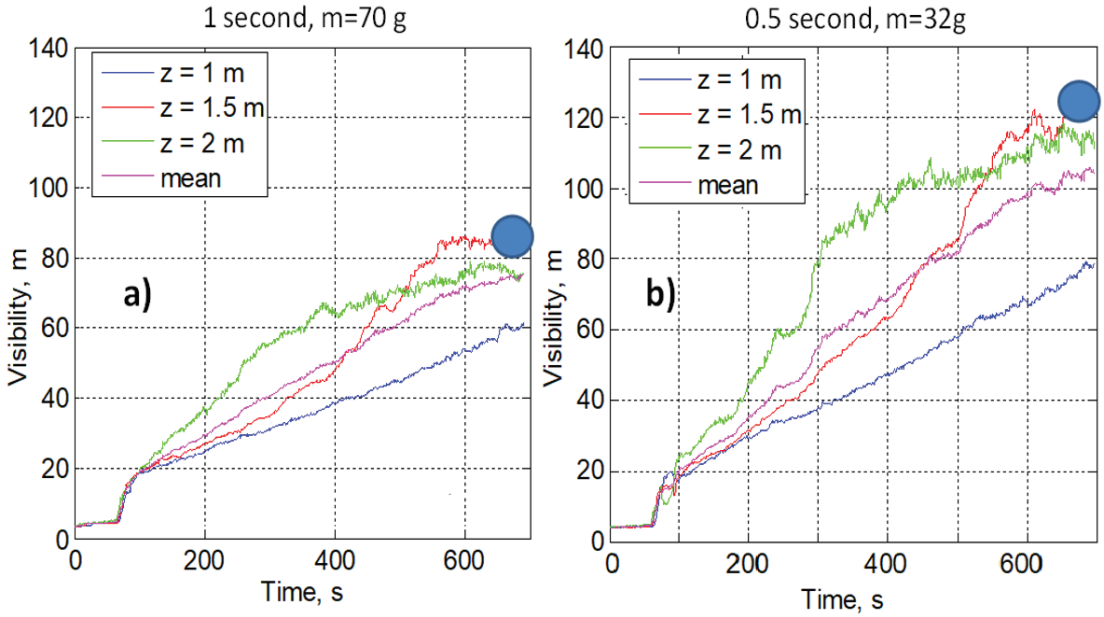

Fig. 6. Time dependencies of visibility in experiments with $MgCl_2$ seeding drops and seeding durations of 1 s (a) or 0.5 s (b). Total seeding mass were 70 g (a) and 32 g (b). Dots show the most presentable results.

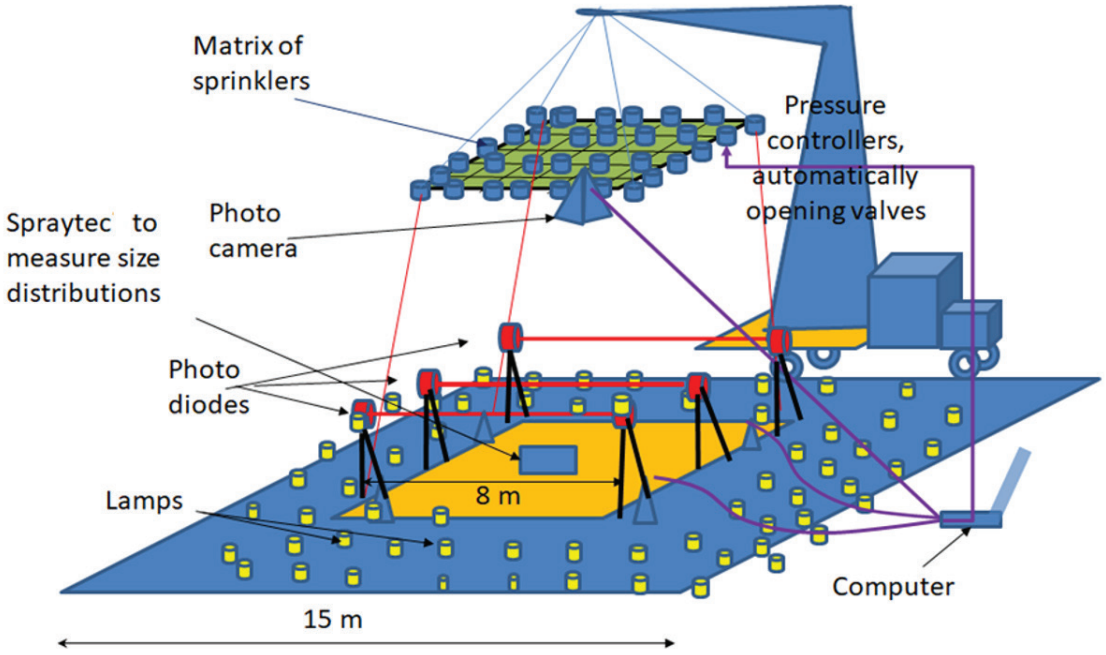

Fig. 7. A scheme of the field experiment setup.

suspended on a truck crane and could be raised up to a height of 10 m. Below the matrix, 3 optical transmissometers were positioned at height of 1.5 m. The transmissometers were used to measure visibility under foggy and background radiation conditions. Accordingly, all optics were purged with fresh air to prevent condensation on surfaces. Furthermore, diode laser intensities were modulated at 129 Hz, and the signal/ref avalanche photodetectors were recorded through A/D card equipped with LabView lock-in amplifier software kit. With this homodyne detection, it was possible to measure very low visibility (0.5 m) and signal variations with a time resolution of 1 s during seeding.

In the center of the area, below the sprinkler matrix, the Spraytec was positioned to measure the salty drop size distribution.

It was recognized that wind fluctuations could shift the seeded air volume outside the zone below the matrix. Accordingly, we selected for the field experiment a valley area in the region of Bet Zait near Jerusalem, where the wind is low. Fog often rises in this area during the cold season in Israel. Since the fog was of a radiative nature, it formed during the nighttime, when heat loss through radiation lowers the temperature and increases the relative humidity, resulting in formation of fog. The line of sight of the transmissometers was designed in such a way that each transmissometer was able to detect fog elimination near the ground. Lamps were installed on the ground to illuminate the experimental area and the sprinkled seeding drops.

The visibility, humidity, temperature, and wind were monitored near the experimental zone a couple of months before the experiment, aiming to evaluate typical meteorological conditions during fog events. It was found that fog events were comparatively frequent during the nighttime in this place when the wind speed was below 0.5 m/s. Visibility (measured at a slightly higher location) often decreased below 500 m, indicating the presence of fog much lighter than that in the fog chamber. The carrying out of the field experiment required successful prediction of the fog and its parameters, such as the strength and direction of the wind near the surface, visibility, and other characteristics. Note that the radiation

fog occurs at night time, which complicated the preparation and conduction of the experiment. Therefore, the forecast had to be given at least two days in advance.

Note that there are no accurate schemes of fog prediction at present. Accordingly, a special fog forecast scheme has been developed with help of the operative weather forecast COSMO (Consortium for Small-scale Modeling) of the Israel Meteorological Service. This model had a spatial resolution of 2.8 km. The results of the model forecasts of wind, temperature and humidity for several past years and a historical set of fog measurements in this area were used to develop regression equations related to the weather forecast and fog appearance to predict fog events up to three days in advance. The fog forecast scheme has been tested for current real forecasts and showed very good results. In case that several 6-h successive forecasts predicted fog in advance of 36-48 h, the fog took place. The development of such a prediction scheme and the provision of regular (every 6 h) fog forecasts were crucial for the field experiment. After a long period without fog in February and early March, a fog of reasonable intensity was predicted for the night of 13 March 2018, during which the experiment was carried out. Images of the fog in the experimental area in the early morning hours of 13 March 2018, at the end of the experiment, are presented in Fig. 8.

An overview of the entire experimental setup is presented in Fig. 9. One can see that it corresponds to the scheme shown in Fig. 7.

Carrying out the experiment. An NaCl water solution with a mass salinity of 20% was prepared. The size distributions of the seeding drops under various pressures in the sprinklers and at different heights were measured by the Spraytec particle size analyzer at the start of the seeding experiment (Fig.

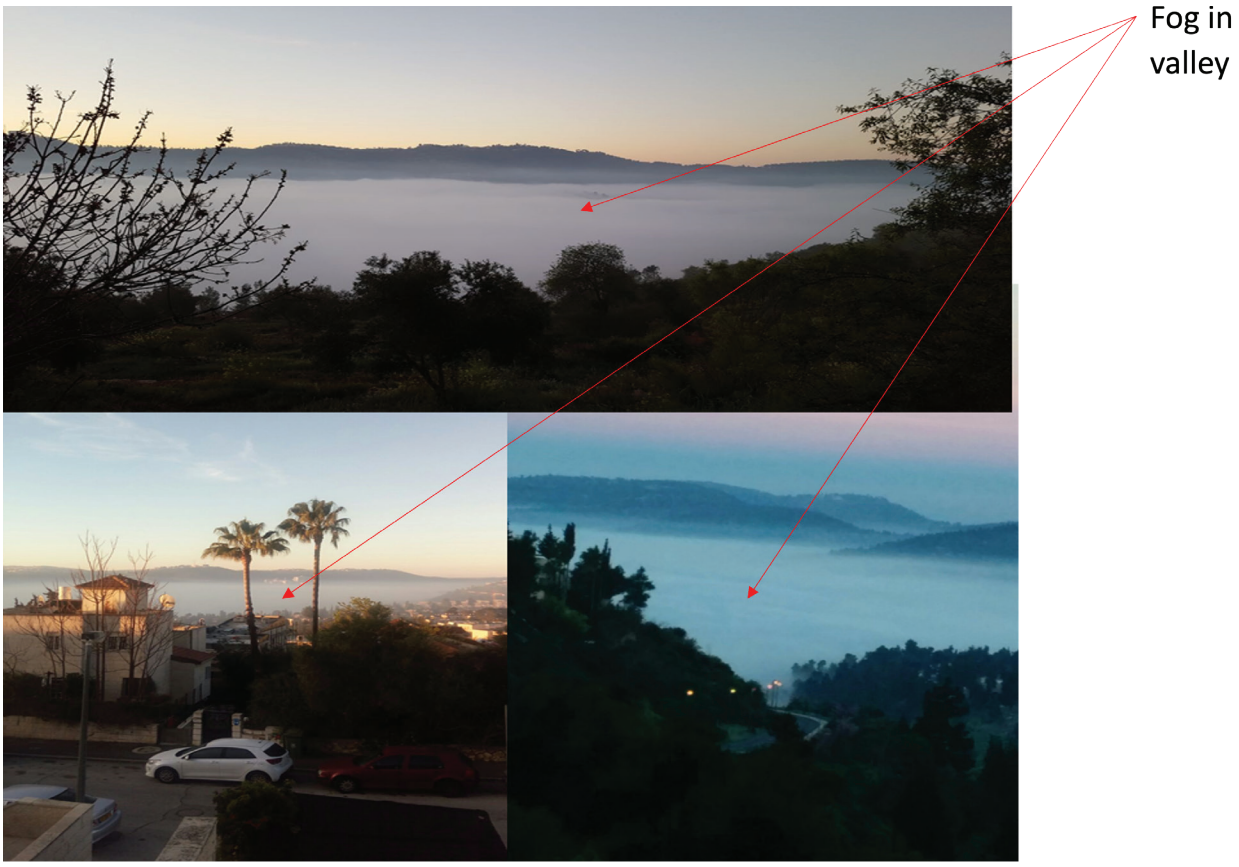

Fig. 8. Photos of the fog in the experiment area during the early morning hours of 13 March 2018, at the end of the experiment.

Fig. 9. A view of the experimental setup.

10) before the fog appeared. One can see that the size distributions were wide, i.e., they contained small and large drops. The distribution width was at its maximum at a pressure of 5.5 atm. Salty drops were seeded from a height of 10 m and exhibited the largest sizes (green curve), supposedly because the smallest seeding drops were advected by the wind and did not reach the Spraytec positioned on the ground. The characteristic seeding drops diameter was 100–200 μm, close to the drop sizes used in the laboratory experiment.

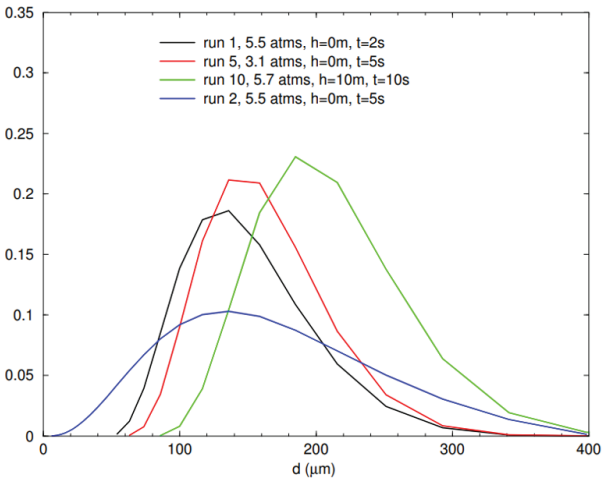

Fig. 10. Normalized size distributions of salty drops at various pressures, ejection durations, and heights. These distributions were measured during individual seeding runs.

Subsequently, fog seeding was performed. Several parameters were changed during the seeding experiments, including the seeding drop size, matrix height (3.5 and 10 m), and seeding pulse duration (from 2 to 10 s). We used an NaCl 20% solution in all cases. Following, we will present a few examples of typical results for the fog elimination effect.

The seeding drops during fog seeding are shown in Fig. 11. It is apparent that the notable lateral wind present moved the seeded volume from below the matrix, where the transmissometers were installed. Consequently, only some seeded drops reached the transmissometers.

Proof of concept. We present several examples that clearly confirm the desired effect of increased visibility after seeding with salty drops. Fig. 12 shows the time dependency of visibility measured by the three transmissometers before, during, and after seeding in experiment 1. The seeding height (H) was 10 m, duration was 10 s, and pressure was 5.5 atm. The total seeded volume was 876 mL. The mean wind direction was south, so the northernmost transmissometers (Vis3; blue curve) shows the background visibility as it was not affected. Thus, it

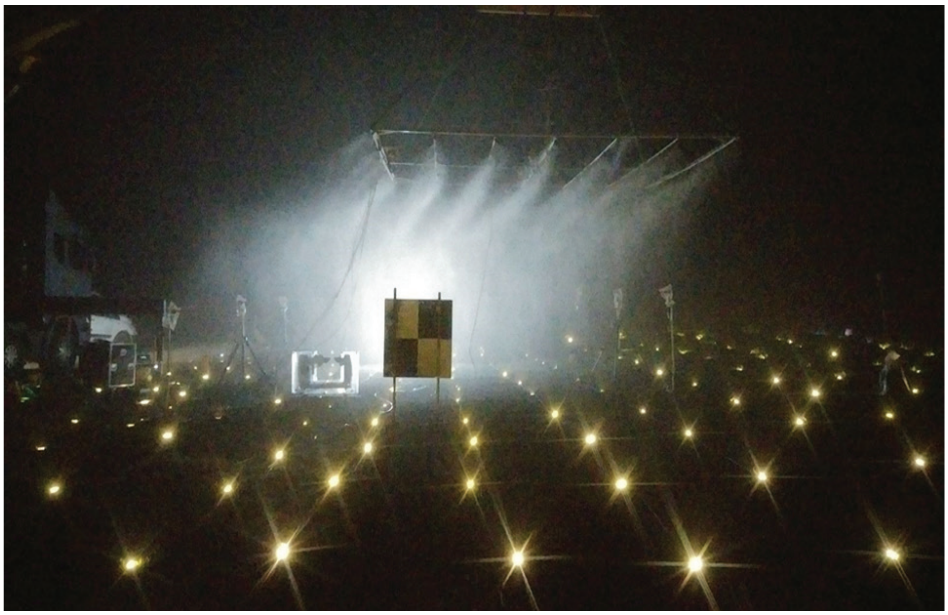

Fig. 11. A photo made during the seeding operation. Seeding salty drops are clearly seen below the matrix. One can see that the seeding drops are transported to the left by the background wind.

can be regarded as the background visibility during this measurement. The other two transmissometers show the initial decrease in visibility caused by the seeding drops. Thereafter, visibility measured by the central (Vis2) and southern (Vis1) transmissometers increased, particularly in the zone of Vis1. Visibility exceeded 300 m, more than twice the background visibility, and its peak lasted about 1 min. Using the time shift between visibility peaks (see red and black curves), we estimated the wind speed at 20 cm/s which agreed with the wind measurements. The wind speed and direction continuously changed because of turbulent fluctuations.

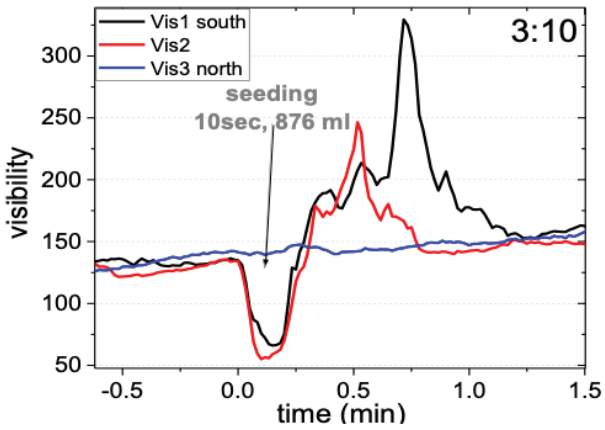

Fig. 12. Time dependence of visibility measured by three photo sensors in experimental run 1. The mean wind direction was south, so the northernmost photo sensor was unaffected. The southern photo sensor was within the seeded volume for the longest time. Vis1, Vis2 and Vis3 denote 3 transmissometers. 3:10 is the local time of measurements.

Fig. 13 shows the seeding effects on visibility in experiment 2 (H = 3.5 m; seeding duration, 5 s; seeding pressure, 2.2 atm). The central transmissometer shows the initial decrease in visibility caused by the seeding drops. It seems that clean air passed only over the northern transmissometer, which showed increased visibility.

A more spectacular effect of seeding was seen in experiment 3 (H = 3.5 m; seeding duration, 10 s; seeding pressure, 5.4 atm), as illustrated in Fig. 14. Again, we saw an initial decrease in visibility registered by the transmissometers. Thereafter, the seeded volume moved through the laser line of sight of the northern transmissometer, which showed an increase in visibility by a factor of two (from 150 to 300 m) for a significant duration (2 min). This strong effect could be attributed to the low seeding height, from which a higher mass of seeding drops reached the transmissometers.

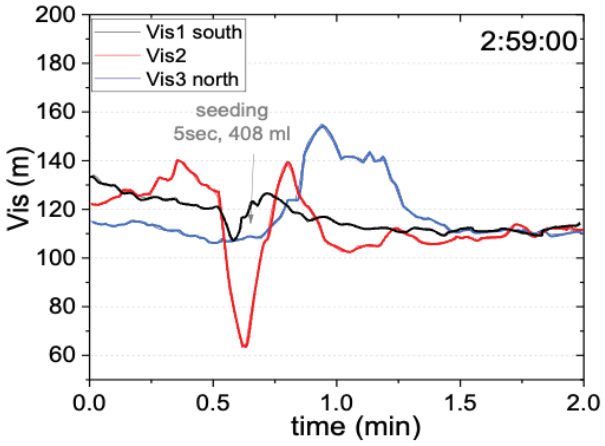

Fig.13. Time dependencies of visibility in Example 2. The mean wind direction was north (changes in the wind direction were caused by turbulence). The northern transmissometer (Vis3) indicated a significant increase in visibility (Vis). The southern transmissometer (Vis1) shows a background visibility of 120 m. Spray ejection was done from a height (H) of 3.5 m, for a duration of 5 s, and at a pressure of 2.2 atm.

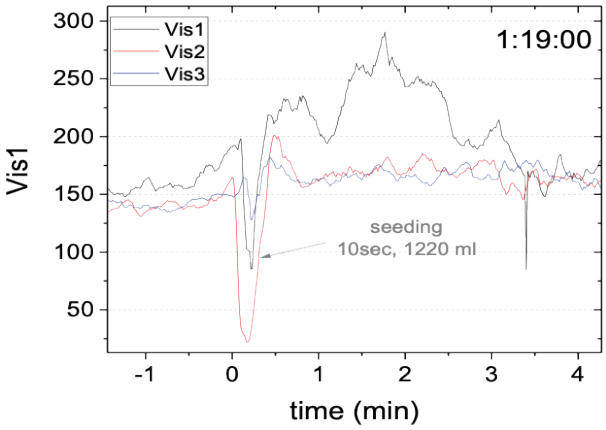

Fig. 14. Time dependence of visibility measured by three photo sensors in experiment 3. The mean wind direction was north, so the northernmost transmissometer (Vis3) was substantially influenced. Seeding conditions: height (H) = 3.5 m; seeding duration, 10 s; ejection pressure, 5.4 atm.

Note that seeding did not affect visibility in experiments with a short seeding duration (3 s). This could be because the spray mass ejected during 3 s was insufficient to evaporate the fog, since only a fraction of the seeding drops reached the transmissometers in the presence of wind.

The results presented in Figs. 12–14 show that:

- Visibility increased after seeding natural fog under natural turbulent flow.
- Seeding effects were typically seen when large drops were used for seeding. This could be because larger drops fell faster and were shifted by the wind to a shorter distance.
- An increase in the seeding duration led to a large increase in visibility. This effect we attribute to the experimental design; seeding drops may not have reached the transmissometers during short seeding pulses because of turbulent velocity fluctuations.

3.0 FOG SEEDING MODELING

Although there is a simple physical explanation behind the method presented above and the interpretation of the experimental results, the interaction of two sets of drops with different salinities (large strongly salty spray and small low salty fog droplets) represents a complicated theoretical and numerical problem. Only theoretical analysis can find the key to the optimal seeding regimens under various environmental conditions. Below we present the description and results of a zero-dimensional mathematical model that describes the physics of the interaction between the seeding drops and the fog droplets. The model closely represents the fog chamber described above.

Model description. We considered two monodisperse sets of drops, fog droplets with a radius r and seeding drops with a radius R, initially located within the same volume. The fog droplets contained dissolved aerosol particles with radii r_n, while the radius of the dissolved salt in the seeding drops was R_n. The r_n values were assumed to be small (0.05 μm), so the fog droplets before seeding were in thermodynamic equilibrium with environment supersaturation, as described by the Kohler equation (Khain and Pinsky, 2018) (1):

$$S - \frac{A}{r} + \frac{Br_n^3}{r^3 - r_n^3} = 0 \qquad (1)$$

where S is supersaturation over water, and A and B are coefficients in the Kohler equation (see Table 1 for notations).

The terms $\frac{A}{r}$ and $\frac{Br_n^3}{r^3-r_n^3}$ describe the effects of curvature and chemical composition on haze/drop growth and evaporation. We also assumed that supersaturation in the volume before seeding was equal to zero (S_o = 0, i.e., RH = 100%). We denoted the initial fog droplet radius r_o and their concentration n. Under this condition, the initial radius of fog droplets (or haze) and aerosol particles are related by equation (2) (Pruppacher and Klett, 1997):

$$r_0 = \sqrt{\frac{B}{A}} r_n^{3/2} \tag{2}$$

The salty seeding drops had an initial radius R_o and concentration N. The initial radii and concentrations of the fog droplets and seeding drops satisfied these inequalities:

$$R_0^3 >> r_0^3; \quad n >> N \tag{3}$$

The time evolution of fog droplets, seeding drops, and supersaturation is described by the following equations (Khain and Pinsky, 2018):

$$r\frac{dr}{dt} = \frac{1}{F}\left(S(t) - \frac{A}{r} + \frac{Br_n^3}{r^3-r_n^3}\right) \tag{4}$$

$$R\frac{dR}{dt} = \frac{1}{F}\left(S(t) - \frac{A}{R} + \frac{BR_n^3}{R^3-R_n^3}\right) \tag{5}$$

$$\frac{1}{S+1}\frac{dS}{dt} = -A_2\left(\frac{dq}{dt} + \frac{dQ}{dt}\right) \tag{6}$$

where (7) $q = \frac{4}{3}\pi\rho_w n(r^3 - r_n^3)$; $Q = \frac{4}{3}\pi\rho_w N(R^3 - R_n^3)$

are liquid water contents (LWCs) of fog droplets and seeding drops, respectively. For simplicity, we assumed that the chemical compositions (NaCl) of fog droplets and seeding drops were similar, so we used the same coefficient B value in Eqs. (4) and (5). Since seeding drops salinity was higher than that of the fog droplets (i.e., $\frac{R_n^3}{R^3-R_n^3} > \frac{r_n^3}{r^3-r_n^3}$), one can expect that the large seeding drops will grow (i.e., $\frac{dR}{dt} > 0$). As a result, $\frac{dQ}{dt}$ will be positive and, thereby, the supersaturation S will decrease. If S becomes negative and r is not too small, the rates $\frac{dr}{dt}$ and $\frac{dq}{dt}$ will be negative as well [see Eq. (4)], indicating fog evaporation. Therefore, the seeding drops grow partially by absorbing water vapor released during fog droplets evaporation. We expected that a decrease in the fog droplets' size would lead to an increase in visibility.

We calculated the visibility of fog, the visibility caused by seeding drops and the total visibility. Visibility was calculated using the definition of WMO and the Met-Office, where visibility was defined as the length of the atmosphere over which a beam of light travels before its luminous flux is reduced to 5% of its original value (Duthon et al. 2019; Gultepe et al. 2009). Accordingly, the formula used for visibility was $Vis = -\frac{\ln 0.05}{\beta_e} \approx \frac{3}{\beta_e}$, where β_e is the extinction coefficient, calculated as $\beta_e = Q\int \pi r^2 N(r)$, where $N(r)$ is the volume number distribution of drops of a radius r and Q = 2 is the efficiency factor of scattering (Jung and Kim 2007; Petty 2006). The combined extinction coefficient of the fog droplets and seeding drops was calculated as the sum of their corresponding extinction coefficients.

Eqs. (4)-(7) were numerically integrated with time using very small time steps (0.001 s). Fig. 15 shows an example of the temporal evolution of supersaturation, radii of the fog droplets and seeding drops, and visibility in a simulation when a fog droplet at a concentration of n = 1000 cm^{-3} was seeded by drops with a 20 μm radius at a concentration of N = 1 cm^{-3}.

One can see that both the seeding drops and fog droplets tended toward the thermodynamic

equilibrium that occurred 300 s after the process started. Low initial visibility of 5 m was determined for the fog. After seeding, the salty drops grew, and visibility decreased. The final supersaturation, fog droplet and drop radii were

$$S_\infty = -3.14\%;\ r_\infty = 0.97\ \mu m;\ R_\infty = 54.4\ \mu m\ .$$

At $t > 150$ s, the seeding drops determined the total visibility (the blue line is below the green one in Fig. 15c). The fog visibility (Fig 15c, green line) increased to 400 m. In this example, seeding with salty spary increased the total visibility from 10.3 m to 75 m (Fig. 15c, red curve).

These evaluations were obtained while neglecting the sedimentation of the seeding drops. Subsequently, we included the sedimentation of the seeding drops to make the calculations more realistic. Owing to the zero-dimensionality of the model, we used the following simple approximation to calculate the sedimentation. A volume of height H was considered uniformly filled by seeding drops. The fall velocity of the seeding drops V_t was calculated using expressions described by Khain and Sednev (1996). The fall velocity determined the decrease in spray concentration with time while keeping the concentration uniform. The decrease in the seeding drops concentration per dt was determined as

$$dN = -N\frac{V_t}{H}dt\ .$$

A similar approach was used by Koenig (1971).

We present below the results of several numerical simulations to illustrate the main factors affecting visibility. The list and conditions of these simulations are presented in Table 2.

The goal of the first two simulations was to demonstrate the fog evaporation sensitivity to the concentration of seeding drops, that was assumed $N = 10$ cm^{-3} in S.1 and $N = 5$ cm^{-3} in S.2. The results of these simulations are presented in Fig. 16, showing time dependencies of the supersaturation (a,d), fog droplet and seeding drop radii (b,e), and visibility caused by fog, seeding drops, and

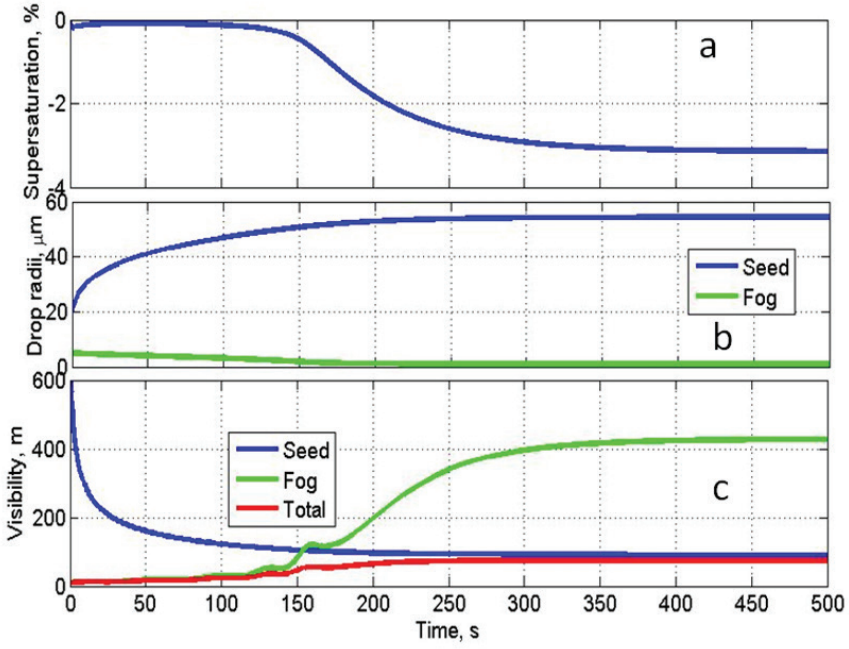

Fig. 15. An example of the temporal evolution of supersaturation (a), radii of the fog droplets and seeding drops (b), and visibility (c). Visibility was calculated for fog, seeding drops, and total. The thermodynamic and initial conditions were: $T = 10$ °C; $p = 950$ mb; $S_0 = 0$; $r_0 = 5$ μm; $r_n = 0.05$ μm; $n = 1000$ cm^{-3}; $R_0 = 20$ μm; $R_n = 15$ μm; $N = 1$ cm^{-3}. Sedimentation of seeding droplets was not included.

TABLE 2. Simulation conditions and the main results.

Simulation Number	Experiment Conditions							Final Visibility Comments
	Fog droplet conc. n, cm^{-3}	Initial fog droplet radius, r_0, μm	Initial fog visibility, m	Conc. of seeding drops, N, cm^{-3}	Initial seeding drop radius R_0, μm	Salt particle radius in seeding drops, R_n, μm	Height of seeding H, m	
S.1	2000	5	3.5	10	100	60	3	High.
S.2	2000	5	3.5	5	100	60	3	15 m. There is a minimal seeding drop concentration.
S.3	500	5	20	2	100	60	3	High. Lower fog concentration requires lower seeding drop concentration.
S.4	500	5	20	2.5	60	36	3	High. Decrease in the seeding drop size decreases the seeding effect. There is a critical seeding drop size.
S.5	100	5	100	0.1	100	60	10	380 m.
S.6	100	5	100	0.2	100	60	10	High.
S.7	100	5	100	0.2	60	36	10	220 m. At the same conditions as S.1, seeding with larger drops is more efficient.
S.8	100	5	100	10	20	12	10	Low visibility: 80 m at t = 100 s. Fog evaporates after 5 s, but seeding particles decrease the visibility.

total visibility (c,f). The conditions of these two simulations were comparable to those used in the fog chamber experiment, with H = 3 m and a seeding drop radius of 100 μm. The only difference between the conditions of the simulations was the difference in the seeding drop concentrations.

The initial visibility, caused by fog, was 3.5 m. This fog was very dense, with an LWC of 2.7 gm^{-3}. The initial total visibility, caused by the combined effects of the fog and seeding drops, was 2.5 m. The seeding drop and fog droplet sizes and the initial salinity of the seeding drops (23%) corresponded to

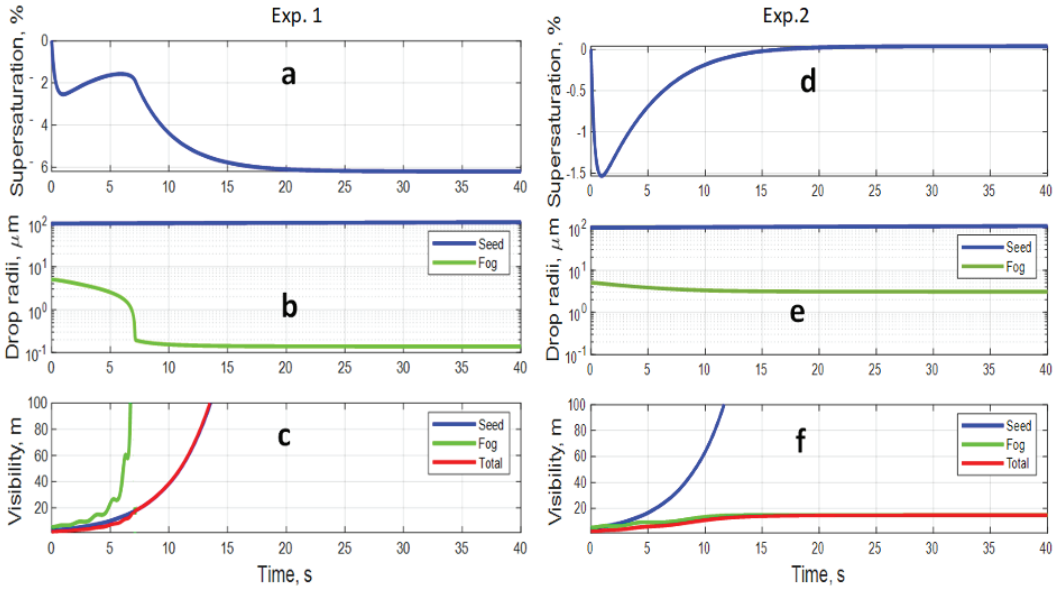

Fig. 16. Time dependencies of supersaturation (a, d), radii of fog droplets and seeding drops (b, e), and visibility affected by the fog droplets, seeding drops, and both combined (total; c, f) in two simulations (S.1) (left column) and S.2 (right column) with conditions comparable to those used in the fog chamber experiment. The conditions of S.1 (a–c) were: H = 3 m; r_0 = 5 μm; r_n = 0.05 μm; n = 2000 cm^{-3}; R_0 = 100 μm; R_n = 60 μm; N = 10 cm^{-3}. The conditions of S.2 (d-f) differed from those of S.1 only in the seeding drop concentration (N = 5 cm^{-3} in S.2). Sedimentation of seeding drops was included.

the laboratory experiment (see Fig. 4). The initial seeding drops mass was 40 gm^{-3} in S.1 and 20 gm^{-3} in S.2.

One can see a dramatic difference between the results of the two experiments. In S.1, supersaturation fell to –6%, and the fog droplet radius decreased from 5 to 0.15 μm (Fig. 16b). As a result, the fog visibility increased within several seconds to very high values, while the total visibility was determined by the seeding drops (Fig. 16c). In contrast, the seeding drops concentration in S.2 was not high enough, so the fog droplet radius only decreased to 3 μm, indicating that relatively large fog droplets remained after all the seeding drops settled. The final visibility (~15 m) was determined by the remaining fog. The solution of S.2 tended to an equilibrium quite different from that in S.1. Therefore, *there is a minimal (critical) seeding drop concentration* needed to evaporate fog and a significantly increase the visibility. When the seeding drops concentration is below this minimum value, the seeding effect on visibility will be insignificant. The result of simulation S.1 resembles those observed in the fog chamber.

The subsequent two numerical simulations aimed to illustrate sensitivity of the seeding effects to the fog droplet concentration (S.3) and the seeding drop size (S.4). In both experiments, the initial fog droplet concentration was 500 cm^{-3} , corresponding to initial visibility of 20 m (Fig. 17). The conditions of the experiments are described in the figure caption. A decrease in the fog droplet concentration from 2,000 cm^{-3} to 500 cm^{-3} led to a decrease in the necessary seeding drop concentration in nearly the same proportion, from 10 cm^{-3} to 2 cm^{-3}. In S.3, total visibility was determined by the fog because drops with a radius of 100 μm sediment fast.

A decrease in the seeding drop radius to 60 μm at the same salinity in S.4 required a seeding drop concentration of 2.5 cm^{-3}. A lower concentration did not lead to any significant increase in visibility. The visibility increase rate in S.4 was determined by the seeding drops, which had a lower fall velocity than drops with a radius of 100 μm. Interestingly, a similar increase in visibility was achieved at H = 3 m with a substantially lower seeding drop concentration (and mass). This was

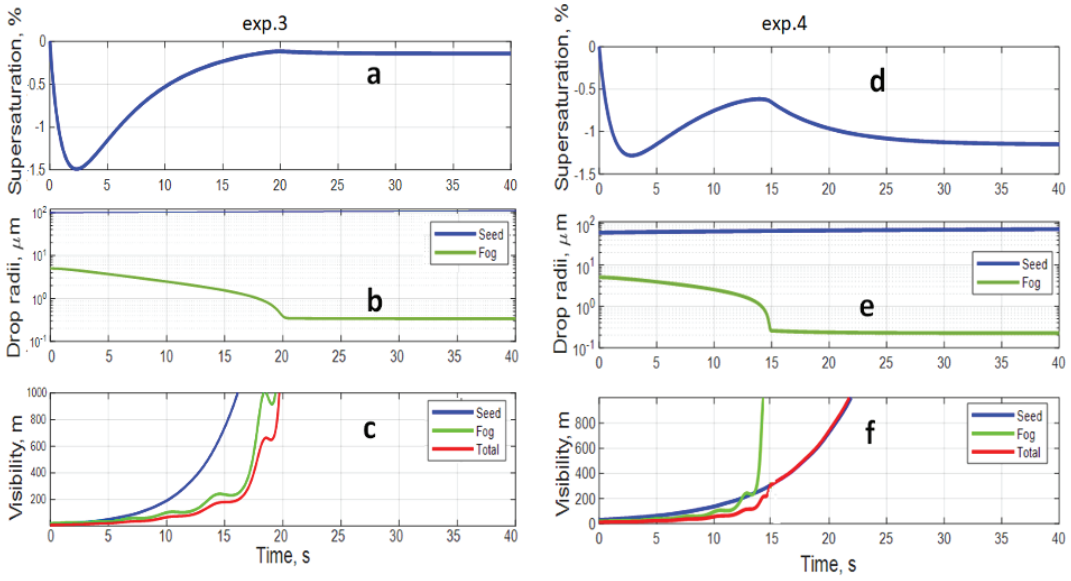

Fig. 17. The same as in Fig. 16, but for simulations S.3 (left column) and S.4 (right column) in the conditions of S.3: $H = 3$ m; $r_0 = 5$ μm; $r_n = 0.05$ μm; $n = 500$ cm^{-3}; $R_0 = 100$ μm; $R_n = 60$ μm; $N = 2$ cm^{-3}. Initial visibility is 20 m. The conditions of S.4 are similar to those in S.3, but $R_0 = 60$ μm; $R_n = 36$ μm; $N = 2.5$ cm^{-3}.

because the 60 μm drops remained longer in the fog, leading to its evaporation. Large drops sedimentation is too fast to evaporate the fog at such a small height. Consequently, a larger concentration of such drops is required to achieve the same effect.

These numerical simulations showed that in the case of the monodisperse size distribution of seeding drops and fog droplets, there are critical values of seeding drop parameters. A small change in these parameters could lead to a dramatically different result (visibility and the final fog droplet size, in our case). Evidently, we have identified the points of bifurcation. In the space of the model parameters (size, mass, and salinity of the fog droplets, the height of seeding, etc.), these critical points form bifurcation surfaces and require an analytic investigation.

Additional simulations showed that a decrease in the seeding drops salinity substantially decreased the fog elimination effect (not shown).

The next four simulations were performed with a seeding height of 10 m and fog droplet concentration of 100 cm^{-3}. This fog concentration resulted in initial visibility of 100 m.

Simulations S.5 and S.6 (Fig. 18) differed in their seeding drop concentrations (0.1 cm^{-3} in S.5 and 0.2 cm^{-3} in S.6). The critical spray concentrations needed to eliminate fog is between 0.1 cm^{-3} and 0.2 cm^{-3}. This critical value separates the two final states because a further decrease in the spary concentration did not increase visibility. At $N = 0.1$ cm^{-3} fog droplet size decreased only from 5 to about 3 μm (Fig 18b). The final visibility of 350 m is determined by the remined fog. The final supersaturation was about zero (Fig 18a). An increase in the seeding drop concentration to $N = 0.2$ cm^{-3} led to the complete evaporation of the fog (Fig 18e). The supersaturation reached its stationary value of ~–0.7% (Fig. 18d). As a result of the fog evaporation, visibility exceeded 600 m already 25 s after seeding (Fig. 18f). This result indicated again the high efficiency of the method when used under an optimal regime. We believe the case in S.5 is close to that in the field experiment, in which the wind decreased the concentration of seeding drops passing through the transmissometers line of sight.

Fig. 18 shows the results of simulations S.7 and S.8. S.7 was similar to S.6, but the seeding drop radius was 60 μm instead of 100 μm. One can see that

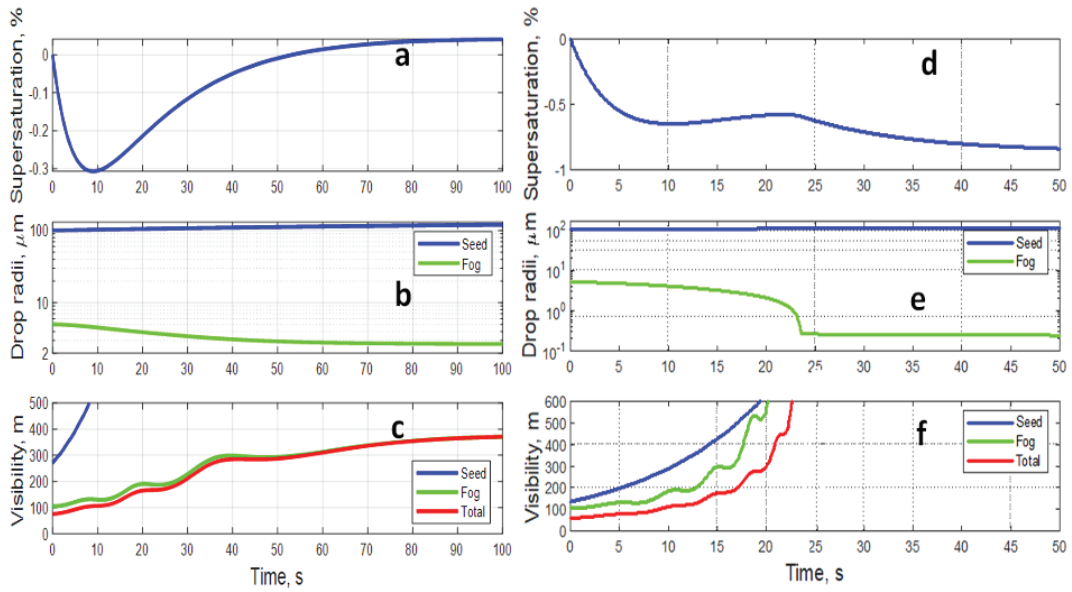

Fig. 18. The same as in Fig. 16, but for simulations S.5 (left column) and S.6 (right column). In both simulations H = 10 m and the initial fog visibility was 100 m. The conditions of S.5 were: r_0 = 5 μm; r_n = 0.05 μm; n = 100 cm^{-3}; R_0 = 100 μm; R_n = 60 μm; N = 0.1 cm^{-3}. The conditions of simulation S.6 (right column) were as in S.5, but with N = 0.2 cm^{-3}.

the final visibility was 220 m instead of more than 600 m in S.6. This result shows that under given conditions, seeding with larger drops is preferable. A comparison with the results of simulations with H = 3 m showed that the larger the H, the larger the optimal seeding drop radius. Small seeding drops with a radius of 20 μm were used in S.8. A seeding drop concentration 50 times higher than in S.6 was needed to evaporate the fog in this case. One can see that these multiple small seeding drops eliminated the fog very rapidly, within 5 s (Fig. 19f), with a decrease in the fog droplet radius from 5 to 0.1 μm

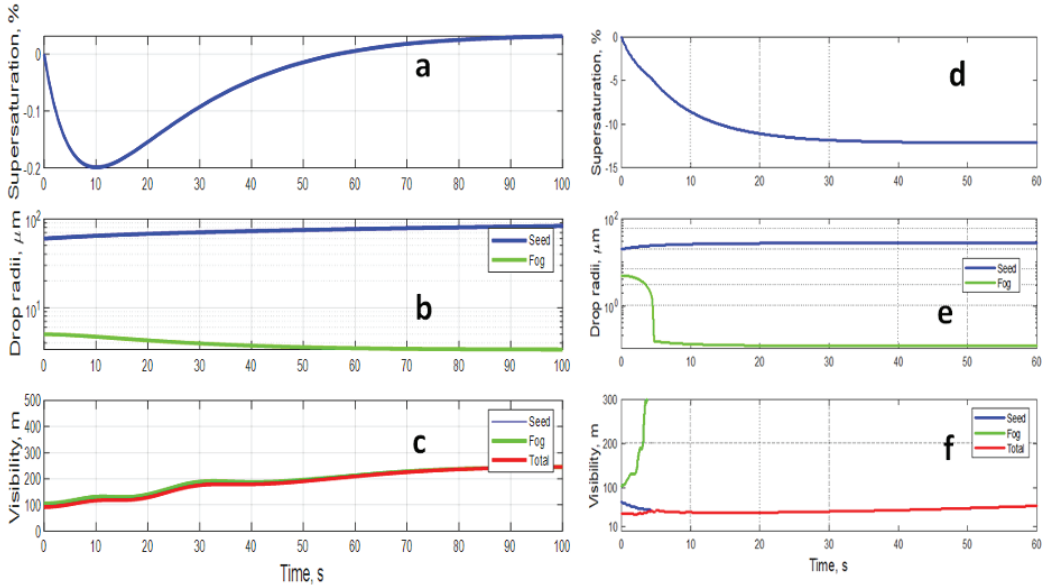

Fig. 19. The same as in Fig. 16, but for simulations S.7 and S.8. Simulation S.7 (a–c), was like S.6, but the seeding drop radius was 60 μm. In simulation S.8 (d-e), the seeding drop radius was 20 μm and concentration 0.2 cm^{-3}.

(Fig. 19e). However, the low sedimentation velocity of these seeding drops led to a decrease in visibility from the initial 100 m to 20–30 m. During time interval of 60 s, the seeding drop radius increased to 28 μm, their salinity decreased from 23 to 12%, and supersaturation was established at –12% (Fig. 19d). An increase in visibility can be expected only after sedimentation of these drops, after 200–250 s in our case. However, under natural conditions, new background fog can enter the seeding zone during this time interval.

4.0 CONCLUSIONS

This study evaluated the efficiency of a fog elimination by seeding with salty drops in a fog chamber and a field experiment and using a zero-dimensional numerical model. The model assumed monodisperse distributions of the fog and seeding particles. The method seems to be efficient, and its application is simple. Fog elimination occurred within several to a few tens of seconds. The seeding material (i.e., salty water) is inexpensive, and its required mass is small and does not represent any ecological problem.

Measurements and theoretical simulations showed that there is an optimal concentration and seeding drop size for any given seeding drop salinity and seeding conditions (fog droplet size and concentration, height of drop seeding, and fog visibility). Advantages of the method over seeding with dry hygroscopic particles include the ability to control and change the seeding drop size (lack of conglomeration) and choose the optimal size suitable for the given conditions. The seeding drops must evaporate the fog and fall to the surface as soon as possible to increase the total visibility. These two requirements determine the optimal size and concentration of the seeding particles. The numerical simulations showed that seeding with small drops like those that can form after seeding with "dry" hygroscopic particles could lead to fog evaporation but require too long time to sediment to the surface. As a result, visibility can even decrease after such seeding. Therefore, seeding with salty drops with a radius of several tens of micrometers has a significant advantage over the seeding with hygroscopic particles. Seeding with large hygroscopic particles having large fall velocity would require a very high mass of seeding material which can lead to ecological problems.

The critical seeding drop size and mass and other seeding parameters like the duration and rate of production can be derived from numerical analysis. The development and utilization of a more complicated multi-dimensional numerical model is required for this. In such a model, the wind speed and turbulence influence should be considered, and the seeding and seeded drop sedimentation process be more realistically described than in the dynamically simple model used in this study. It is also necessary to use realistic multidisperse size distributions of the fog droplets and seeding drops.

Field experiments with drops of various sizes and fog under various meteorological conditions (e.g., different wind speeds) and over larger areas are required to test the method over practically important large fog areas.

5.0 ACKNOWLEDGMENTS

The study was supported by the Israel Science foundation, grants (2635/20, 1449/22). The codes of the model are available by request.

6.0 REFERENCES

Chernikov, A. A., and M. N. Khainkine, 1999: The use of electrical precipitators to clear warm fog. *7th WMO Sci. Conf. on Weather Modification*, Chiang Mai, Thailand.

Duthon, P., M. Colomb, and F. Bernardin, 2019: Light Transmission in Fog: The Influence of Wavelength on the Extinction Coefficient. *Applied Sciences*, **9**, 2843, https://doi.org/10.3390/app9142843.

Frost, W., L. S. Christensen, F. G. Collins, and D. W. Camp, 1980: Fog Dispersion. *Aerospace Congress and Exposition*, Los Angeles Convention Center.

Gultepe, I., and Coauthors, 2009: The Fog Remote Sensing and Modeling Field Project. *Bull. Amer. Meteor. Soc.*, **90**, 341–360, https://doi.org/10.1175/2008BAMS2354.1.

He, H., X. Guo, X. Liu, Q. Gao, and X. Jia, 2016: Mesoscale numerical simulation study of warm fog dissipation by salt particles seeding. *Adv. Atmos. Sci.*, **33**, 579–592, https://doi.org/10.1007/s00376-015-5151-2.

Houghton, H. G., and W. H. Radford, 1938: On the local dissipation of warm fog. *Papers Physical Oceanography Meteorology*, **6**, 63.

Jiusto, J. E., R. J. Pilié, and W. C. Kocmond, 1968: Fog Modification with Giant Hygroscopic Nuclei. *J. Appl. Meteor.*, **7**, 860–869, https://doi.org/10.1175/1520-0450(1968)007<0860:FMWGHN>2.0.CO;2.

Jung, C. H., and Y. P. Kim, 2007: Technical Note: Particle Extinction Coefficient for Polydispersed Aerosol Using a Harmonic Mean Type General Approximated Solution. *Aerosol Science and Technology*, **41**, 994–1001, https://doi.org/10.1080/02786820701644285.

Khain, A. P., and I. Sednev, 1996: Simulation of precipitation formation in the Eastern Mediterranean coastal zone using a spectral microphysics cloud ensemble model. *Atmospheric Research*, **43**, 77–110, https://doi.org/10.1016/S0169-8095(96)00005-1.

Khain, A., V. Arkhipov, M. Pinsky, Y. Feldman, and Y. Ryabov, 2004: Rain Enhancement and Fog Elimination by Seeding with Charged Droplets. Part I: Theory and Numerical Simulations. *Journal of Applied Meteorology*, **43**, 1513–1529, https://doi.org/10.1175/JAM2131.1.

Khain, A. P., and M. Pinsky, 2018: *Physical processes in clouds and cloud modeling*. Cambridge University Press, 626 pp.

Koenig, L. R., 1971: NUMERICAL EXPERIMENTS PERTAINING TO WARM-FOG CLEARING [1]. *Mon. Wea. Rev.*, **99**, 227–241, https://doi.org/10.1175/1520-0493(1971)099<0227:NEPTWC>2.3.CO;2.

Kornfeld, P., 1970: Some Numerical Experiments for Warm Fog Clearing by Seeding with Hygroscopic Nuclei. *J. Appl. Meteor.*, **9**, 459–463, https://doi.org/10.1175/1520-0450(1970)009<0459:SNEFWF>2.0.CO;2.

Kunkel, B. A., and B. A. Silverman, 1970: A Comparison of the Warm Fog Clearing Capabilities of Some Hygroscopic Materials. *J. Appl. Meteor.*, **9**, 634–638, https://doi.org/10.1175/1520-0450(1970)009<0634:ACOTWF>2.0.CO;2.

Mather, G. K., D. E. Terblanche, F. E. Steffens, and L. Fletcher, 1997: Results of the South African Cloud-Seeding Experiments Using Hygroscopic Flares. *J. Appl. Meteor.*, **36**, 1433–1447, https://doi.org/10.1175/1520-0450(1997)036<1433:ROTSAC>2.0.CO;2.

Petty, G. W., 2006: *A First Course in Atmospheric Radiation*. Sundog Publishing, 452 pp.

Pruppacher H. R., Klett J. D., 1997: *Microphysics of Clouds and Precipitation.* Kluwer Academic Publishers, Dordrecht/Boston/London, 954 pp.

Reuge, N., P. Fede, J.-F. Berthoumieu, F. Foucoin, and O. Simonin, 2017: Modeling of the Denebulization of Warm Fogs by Hygroscopic Seeding: Effect of Various Operating Conditions and of the Turbulence Intensity. *Journal of Applied Meteorology and Climatology*, **56**, 249–261, https://doi.org/10.1175/JAMC-D-16-0151.1.

Segal, Y., A. Khain, M. Pinsky, and D. Rosenfeld, 2004: Effects of hygroscopic seeding on raindrop formation as seen from simulations using a 2000-bin spectral cloud parcel model. *Atmospheric Research*, **71**, 3–34, https://doi.org/10.1016/j.atmosres.2004.03.003.

Silverman, B. A., and B. A. Kunkel, 1970: A Numerical Model of Warm Fog Dissipation by Hygroscopic Particle Seeding. *J. Appl. Meteor.*, **9**, 627–633, https://doi.org/10.1175/1520-0450(1970)009<0627:ANMOWF>2.0.CO;2.

Silverman, B. A., and T. B. Smith, 1971: A Computational an Experimental Program in Warm Fog Mitigation. *Proceedings of the Second Conference on Weather Modification*, Santa Barbara, California, 108–111.

Weinstein, A. I., and B. A. Silverman, 1973: A Numerical Analysis of Some Practical Aspects of Airborne Urea Seeding for Warm Fog Dispersal at Airports. *J. Appl. Meteor.*, **12**, 771–780, https://doi.org/10.1175/1520-0450(1973)012<0771:ANAOSP>2.0.CO;2.

Zhao, Q. Y., 1989: Numerical simulation of warm fog dissipation by salt-seeding. *Journal of Tropical Meteorology*, **5** (3), 245–252 (in Chinese).

APPENDIX

TABLE 1. List of symbols ("nd" means non-dimensional).

Symbol	Description	Units
A	$\frac{2\sigma_w}{\rho_w R_v T}$, coefficient	m
B	$\frac{\nu_N \Phi_s \delta_s M_w \rho_N}{M_N \rho_w}$, coefficient	nd
A_2	$\frac{1}{\rho_v} + \frac{L_w^2}{c_p R_v T^2 \rho_a}$, coefficient	nd
σ_w	The surface tension coefficient	N m^{-2}
ρ_w	Water density	Kg m^{-3}
ρ_N	Density of dry aerosol particle	Kg m^{-3}
R_v	Specific gas constant of water vapor	J $kg^{-1}K^{-1}$
L_w	latent heat for liquid water	J kg^{-1}
N	Seeding drop concentration	m^{-3}
T	temperature	K
q	liquid water mixing ratio of fog	kg/kg
Q	liquid water mixing ratio of seeding drops	kg/kg
V_N	The total number of ions produced by one salt molecules	nd
Φ_s	The molecular osmotic coefficient	nd
M_w	Molecular mass of water	kg/ml
M_N	Molecular mass of salt	kg/ml
δ_s	Soluble fraction of aerosol particle	nd
r_n	Radius of aerosol in fog droplets	m
R_n	Radius of fog droplets	m
r	Radius of aerosol in salty drops	m
R	Radius of salty drops	m
S	$e / e_w - 1$, supersaturation over water	nd
e	Water vapor pressure	kg m^{-2}
e_s	Saturated water vapor pressure	kg m^{-2}